
MULTI-SOURCE DOMAIN ADAPTATION THROUGH DATASET DICTIONARY LEARNING IN WASSERSTEIN SPACE

Eduardo Fernandes Montesuma
CEA, List
Université Paris-Saclay
F-91120 Palaiseau, France

Fred Ngolè Mboula
CEA, List
Université Paris-Saclay
F-91120 Palaiseau, France

Antoine Souloumiac
CEA, List
Université Paris-Saclay
F-91120 Palaiseau, France

ABSTRACT

This paper seeks to solve Multi-Source Domain Adaptation (MSDA), which aims to mitigate data distribution shifts when transferring knowledge from multiple labeled source domains to an unlabeled target domain. We propose a novel MSDA framework based on dictionary learning and optimal transport. We interpret each domain in MSDA as an empirical distribution. As such, we express each domain as a Wasserstein barycenter of dictionary atoms, which are empirical distributions. We propose a novel algorithm, DaDiL, for learning via mini-batches: (i) atom distributions; (ii) a matrix of barycentric coordinates. Based on our dictionary, we propose two novel methods for MSDA: DaDiL-R, based on the reconstruction of labeled samples in the target domain, and DaDiL-E, based on the ensembling of classifiers learned on atom distributions. We evaluate our methods in 3 benchmarks: Caltech-Office, Office 31, and CRWU, where we improved previous state-of-the-art by 3.15%, 2.29%, and 7.71% in classification performance. Finally, we show that interpolations in the Wasserstein hull of learned atoms provide data that can generalize to the target domain¹.

 <https://github.com/eddardd/demo-dadil/>

Keywords Optimal Transport · Transfer Learning · Domain Adaptation · Dictionary Learning

1 Introduction

Traditional Machine Learning (ML) works under the assumption that training and test data follow a single probability distribution. Indeed, the Empirical Risk Minimization (ERM) framework of [37] measures generalization regarding an unknown probability distribution from which training and test data are sampled. Nonetheless, as [25] remarks, this is seldom the case in realistic applications due to changes in how the data is acquired. This results in a change in the data distribution, or distributional shift that motivates the field of Domain Adaptation (DA).

DA is an important framework where one assumes labeled data from a source domain and seeks to adapt models to an unlabeled target domain. When multiple source domains are available, one has a Multi-Source DA (MSDA) setting. This problem is more challenging as one has multiple distributional shifts co-occurring, that is, between sources and between sources and the target. In this work, we assume that the domain shifts have regularities that can be learned and leveraged for MSDA. In this context, Optimal Transport (OT) is a mathematical theory useful for DA, as it allows for the comparison and matching probability distributions. Previous works employed OT for the single-source case, as in [1, 2, 3], and MSDA as in [4, 5, 6].

In parallel, Dictionary Learning (DiL) expresses a set of vectors as weighted combinations of dictionary elements, named atoms. Previous works proposed OT for DiL over histogram data, such as [7] and [8]. Nonetheless, when data is high-dimensional, modeling distributions as histograms is intractable due to the curse of dimensionality, which limits the use of previous DiL works for MSDA.

¹Accepted as a conference paper at the 26th European Conference on Artificial Intelligence

Contributions. In this paper we propose a novel DiL framework (section 4), for distributions represented as point clouds. We further explore (section 4.2) two ways of using DiL for MSDA, by reconstructing labeled samples in the target domain, and by ensembling classifiers learned with labeled data from atoms. In addition, we justify these methods theoretically through results in the literature [9, Theorem 2], and through novel theoretical results (i.e., theorem 2). To the best of our knowledge this is the first work to propose a DiL of point clouds, and to explore the connections between DiL of distributions and MSDA.

Paper Organization. Section 2 covers the related literature. Section 3 covers the necessary background, i.e., DA, OT and DiL concepts. Section 4 presents our framework. Section 5 explores our experiments in MSDA. Section 6 discusses our results. Finally, section 7 concludes our paper.

2 Related Work

There are mainly two methodologies in DA. The first, shallow DA, leverages pre-existing feature extractors and performs adaptation either by re-weighting or transforming source domain data to resemble target domain data. The second, deep DA, uses source and target domain data during the training of a Deep Neural Net (DNN), so that learned features are independent of distributional shift.

There are at least 3 classes of shallow DA methods: (i) importance re-weighting strategies [10], which give importance to source samples similar to the target domain, (ii) projection-based methods [11], which seek a sub-space where distributions share common characteristics, and (iii) OT-based methods [1], which use OT for matching, or calculating distances between distributions.

For deep DA, methods penalize encoder parameters that map source and target distributions to different locations in the latent space. As a consequence, deep DA is more complex than shallow DA, since encoder parameters are free. Examples of deep DA methods include [12], who uses an adversarial loss, and [3, 13], who use OT as a loss function between distributions of latent representations.

For MSDA, some works generalize previous single-source baselines. For instance, [14] proposes a moment-matching strategy across the different domains. [6] proposes weighting source domains linearly, then applying the Joint Distribution Optimal Transport (JDOT) strategy of [2]. This approach combines notions of importance weighting and OT-based DA. [4, 5] generalize the approach of [1], by first calculating a Wasserstein barycenter of the different source domains, then transporting the barycenter to the target domain.

In parallel, DiL is a representation learning technique, that was previously used in DA by [15]. However, classic DiL lacks a probabilistic interpretation. In this context, OT offers a probabilistic foreground for DiL, when data is represented through histograms. This is done by either using the Sinkhorn divergence [16] as the objective function [7], or by aggregating atoms in a Wasserstein space [8]. Nonetheless, in the context of DA it is computationally intractable to bin the feature space, which is commonly high-dimensional. This issue hinders the applicability of previous DiL approaches for DA. In contrast, we propose a new OT-inspired DiL framework for point clouds, which makes it suitable for MSDA.

3 Background

3.1 Domain Adaptation

In ML, learning a classifier consists on estimating $h : \mathcal{X} \rightarrow \mathcal{Y}$, among a set of functions \mathcal{H} , where \mathcal{X} (e.g., \mathbb{R}^d) is the *feature space* and \mathcal{Y} (e.g., $\{1, \dots, n_c\}$) is the *label space*. This estimation is done via *risk minimization* [17],

$$h^* = \operatorname{argmin}_{h \in \mathcal{H}} \mathcal{R}_Q(h) = \mathbb{E}_{\mathbf{x} \sim Q} [\mathcal{L}(h(\mathbf{x}), h_0(\mathbf{x}))], \tag{1}$$

for a loss function \mathcal{L} , a distribution Q , and a ground-truth labeling function h_0 . \mathcal{R}_Q is known as *true risk*. Since Q and h_0 are seldom known *a priori*, it is unfeasible to directly minimize equation 1. In practice, one acquires a *dataset*, $\{(\mathbf{x}_i^{(Q)}, y_i^{(Q)})\}_{i=1}^n$, with $\mathbf{x}_i^{(Q)} \stackrel{\text{i.i.d.}}{\sim} Q$ and $y_i^{(Q)} = h_0(\mathbf{x}_i^{(Q)})$ and minimizes the *empirical risk*,

$$\hat{h} = \operatorname{argmin}_{h \in \mathcal{H}} \hat{\mathcal{R}}_Q(h) = \frac{1}{n} \sum_{i=1}^n \mathcal{L}(h(\mathbf{x}_i^{(Q)}), y_i^{(Q)}).$$

Henceforth $\mathbf{x}_i^{(Q)}$ denotes a feature vector sampled from the marginal $Q(X)$. Likewise, $y_i^{(Q)}$ denotes its corresponding label. We denote its corresponding one-hot encoding (hard-labels) or probability vector (soft-labels) by $\mathbf{y}_i^{(Q)}$.

As discussed in [18], if training and test data are i.i.d. from Q , $\mathcal{R}_Q \rightarrow \hat{\mathcal{R}}_Q$ as $n \rightarrow \infty$. Nonetheless this assumption is restrictive, as it disregards the distributional heterogeneity within training data, and between train and test data, which motivates DA [11]. Following [11], a domain $\mathcal{D} = (\mathcal{X}, Q(X))$ is a pair of a feature space, and a feature distribution. In DA, one has different domains, i.e., a labeled source \mathcal{D}_S with samples $\{(\mathbf{x}_i^{(Q_S)}, y_i^{(Q_S)})\}_{i=1}^{n_{Q_S}}$ and a target \mathcal{D}_T with samples $\{\mathbf{x}_j^{(Q_T)}\}_{j=1}^{n_{Q_T}}$. In practice, one assumes a shared feature space (e.g., \mathbb{R}^d), so that domains differ in their distribution, $Q_S(X) \neq Q_T(X)$. This is known in the literature as *distributional shift*. The goal of DA is improving performance on the target, given knowledge from the source domain. We investigate MSDA, that is, DA between labeled sources $\{\mathcal{D}_{S_\ell}\}_{\ell=1}^{N_S}$ and an unlabeled target \mathcal{D}_T .

3.2 Optimal Transport

OT is a field of mathematics widely used in DA and ML. Henceforth we focus on computational OT. We refer readers to [19] and [20] for further background on this topic. Let $\mathbf{x}_i^{(P)}$ i.i.d. P (resp. $\mathbf{x}_j^{(Q)}$ i.i.d. Q). We P and Q empirically using mixtures of Dirac deltas,

$$\hat{P}(\mathbf{x}) = \frac{1}{n_P} \sum_{i=1}^{n_P} \delta(\mathbf{x} - \mathbf{x}_i^{(P)}). \quad (2)$$

We refer to \hat{P} as a point cloud, and $\mathbf{X}^{(P)} = [\mathbf{x}_1^{(P)}, \dots, \mathbf{x}_{n_P}^{(P)}] \in \mathbb{R}^{n_P \times d}$ to its *support*. The Kantorovich formulation of OT seeks an OT plan, $\pi \in \mathbb{R}^{n_P \times n_Q}$ that *preserves mass*,

$$\Pi(\hat{P}, \hat{Q}) := \left\{ \pi : \sum_i \pi_{i,j} = 1/n_Q; \sum_j \pi_{i,j} = 1/n_P \right\},$$

where $\pi_{i,j}$ denotes how much mass $\mathbf{x}_i^{(P)}$ sends to $\mathbf{x}_j^{(Q)}$. In this sense, the OT problem between \hat{P} and \hat{Q} is,

$$\pi^* = \text{OT}(\mathbf{X}^{(P)}, \mathbf{X}^{(Q)}) = \underset{\pi \in \Pi(\hat{P}, \hat{Q})}{\text{argmin}} \langle \mathbf{C}, \pi \rangle_F, \quad (3)$$

where $\langle \cdot, \cdot \rangle_F$ denotes the Frobenius inner product and $C_{i,j} = c(\mathbf{x}_i^{(P)}, \mathbf{x}_j^{(Q)})$ is called *ground-cost matrix*. This is a linear program on the variables $\pi_{i,j}$, which has computational complexity $\mathcal{O}(n^3 \log n)$. Given π , one often wants to map samples from P into Q , which can be done through the *barycentric projection* [1],

$$T_\pi(\mathbf{x}_i^{(P)}) = \underset{\mathbf{x} \in \mathbb{R}^d}{\text{argmin}} \sum_{j=1}^{n_Q} \pi_{i,j} c(\mathbf{x}, \mathbf{x}_j^{(Q)}).$$

When c is the Euclidean distance, the barycentric projection has closed form,

$$T_\pi(\mathbf{x}_i^{(P)}) = n_P \sum_{j=1}^{n_Q} \pi_{i,j} \mathbf{x}_j^{(Q)}, \quad (4)$$

or $T_\pi(\mathbf{X}^{(P)}) = n_P \pi \mathbf{X}^{(Q)}$ in short.

Optimal Transport for Domain Adaptation. In the seminal works of [1], the authors proposed using OT for DA, under the assumption that there is $T : \mathbb{R}^d \rightarrow \mathbb{R}^d$ such that,

$$T_\# Q_S = Q_T \text{ and } Q_S(Y|X) = Q_T(Y|T(X)), \quad (5)$$

where $T_\#$ is the push-forward operator (see e.g., [21]). [1] propose estimating T through T_π in equation 4, which allows mapping samples from Q_S to Q_T .

Wasserstein Barycenters. When the ground-cost is a distance, OT defines a distance between distributions, $W_c(\hat{P}, \hat{Q}) = \langle \mathbf{C}, \pi^* \rangle_F$, called Wasserstein distance. As such, OT defines barycenters of probability distributions [22]. Henceforth we denote the K -simplex as $\Delta_K = \{\mathbf{a} \in \mathbb{R}_+^K : \sum_k a_k = 1\}$.

Definition 1. For distributions $\mathcal{P} = \{P_k\}_{k=1}^K$ and weights $\alpha \in \Delta_K$, the Wasserstein barycenter is a solution to,

$$B^* = \mathcal{B}(\alpha; \mathcal{P}) = \inf_B \sum_{k=1}^K \alpha_k W_c(P_k, B). \quad (6)$$

Henceforth we call $\mathcal{B}(\cdot; \mathcal{P})$ barycentric operator. In this context, the Wasserstein hull of distributions \mathcal{P} is,

$$\mathcal{M}(\mathcal{P}) = \{\mathcal{B}(\alpha; \mathcal{P}) : \alpha \in \Delta_K\} \quad (7)$$

When the distributions in \mathcal{P} are empirical, solving equation 6 corresponds to estimating the support $\mathbf{X}^{(B)}$ of B . In this context, [23] proposed an algorithm known as *free-support Wasserstein barycenter* for calculating \hat{B} . Let $\mathbf{x}_i^{(B)} \sim \mathcal{N}(\mathbf{0}, \mathbf{I}_d)$ be an initialization for the barycenter’s support. One updates the support of \hat{B} with,

$$\begin{aligned} \pi^{(k,it)} &= \text{OT}(\mathbf{X}^{(P_k)}, \mathbf{X}_{it}^{(B)}) \\ \mathbf{X}_{it+1}^{(B)} &\leftarrow \theta \mathbf{X}_{it}^{(B)} + (1 - \theta) \sum_{k=1}^K \alpha_k T_{\pi^{(k,it)}}(\mathbf{X}_{it}^{(B)}) \end{aligned} \tag{8}$$

where θ is found at each iteration via line search. In the context of MSDA, [4] previously defined a barycenter of labeled distributions by penalizing transport plans $\pi^{(k,it)}$ that mix classes.

Mini-batch OT. For large scale datasets, computing OT is likely unfeasible, due its cubic complexity. A workaround, coming from ML, consists on using mini-batches [24]. For M batches of size n_b , this approach decreases the time complexity to $\mathcal{O}(Mn_b^3 \log n_b)$.

Remark on Notation. While $W_2(\hat{P}, \hat{Q})$ is defined between *empirical distributions*, in practice it is a function of $(\mathbf{X}^{(P)}, \mathbf{X}^{(Q)})$. With an abuse of notation, the mini-batch Wasserstein distance between given random samples of size n_b from P and Q is still noted as $W_2(\hat{P}, \hat{Q})$, with the support matrices restricted to a mini-batch.

3.3 Dictionary Learning

DiL is a representation learning technique that expresses a collection of vectors $\{\mathbf{x}_\ell\}_{\ell=1}^N$, $\mathbf{x}_\ell \in \mathbb{R}^d$ through a set of atoms $\mathcal{P} = \{\mathbf{p}_k\}_{k=1}^K$, $\mathbf{p}_k \in \mathbb{R}^d$ and weights $\mathcal{A} = \{\alpha_\ell\}_{\ell=1}^N$, $\alpha_\ell \in \mathbb{R}^K$. Mathematically,

$$\underset{\mathcal{P}, \mathcal{A}}{\text{argmin}} \frac{1}{N} \sum_{\ell=1}^N \mathcal{L}(\mathbf{x}_\ell, \mathcal{P}^T \alpha_\ell) + \lambda_A \Omega_A(\mathcal{A}) + \lambda_P \Omega_P(\mathcal{P}),$$

where \mathcal{L} is a suitable loss, Ω_A and Ω_P are regularizing terms on \mathcal{A} and \mathcal{P} respectively. In this sense, OT has previously contributed to DiL either by defining a meaningful loss function, or novel ways to aggregating atoms. For instance, [7] proposed using the Sinkhorn divergence of [16] as a loss function, while [8] proposed using Wasserstein barycenters for aggregating atoms. These works assume data in the form of histograms, i.e., $\mathbf{x}_\ell \in \Delta_d$. As consequence, $\mathbf{p}_k \in \Delta_d$ and $\alpha_\ell \in \Delta_K$.

4 Proposed Framework

In this section, we present our novel framework for MSDA, called Dataset Dictionary Learning (DaDiL). As our discussion relies on analogies with DiL theory, we provide in Table 1 a comparison of DiL concepts in different frameworks. In what follows, section 4.1 presents a novel algorithm for computing Wasserstein barycenters of labeled distributions, and section 4.2 presents our framework.

Table 1: Overview of analogies between different frameworks of DiL.

Concept	Symbol	Classic DiL	WDL [8]	DaDiL (ours)
Data	\mathbf{x}_ℓ , or \hat{Q}_ℓ	Vectors	Histograms	Point Clouds
Atom	\mathcal{P}	Vectors	Histograms	Point Clouds
Representation	\mathcal{A}	Vectors	Barycentric Coordinates	Barycentric Coordinates
Reconstruction	\mathcal{B}	Vectors	Histograms	Point Clouds

4.1 Wasserstein Barycenters of Labeled Distributions

We propose a novel algorithm for calculating differentiable Wasserstein barycenters of labeled empirical distributions. This algorithm is at the core of DaDiL (section 4), since we later represent datasets as barycenters of learned atoms.

In OT, there are at least 2 ways of integrating labels, either by penalizing OT plans that transport mass between different classes [1, 4], or by defining a metric in the label space [25]. We choose to integrate labels in the ground-cost,

$$C_{i,j} = \|\mathbf{x}_i^{(P)} - \mathbf{x}_j^{(Q)}\|_2^2 + \beta \|\mathbf{y}_i^{(P)} - \mathbf{y}_j^{(Q)}\|_2^2, \tag{9}$$

where \mathbf{y} denotes labels one-hot encoding, and $\beta > 0$ controls the importance of label discrepancy. While simple, this choice allows us to motivate the barycentric projection of [1], and the label propagation of [26] as first-order optimality conditions of $W_c(\hat{P}, \hat{Q})$,

$$\begin{cases} \hat{\mathbf{x}}_i^{(P)} = T_\pi(\mathbf{x}_i^{(P)}) = n_P \sum_{j=1}^{n_Q} \pi_{i,j} \mathbf{x}_j^{(Q)}, \\ \hat{\mathbf{y}}_i^{(P)} = T_\pi(\mathbf{y}_i^{(P)}) = n_P \sum_{j=1}^{n_Q} \pi_{i,j} \mathbf{y}_j^{(Q)}. \end{cases} \quad (10)$$

Henceforth we denote,

$$\pi = \text{OT}\left((\mathbf{X}^{(P)}, \mathbf{Y}^{(P)}); (\mathbf{X}^{(Q)}, \mathbf{Y}^{(Q)})\right).$$

As a consequence, we can interpolate between two point clouds, since $\hat{\mathbf{y}}_i^{(P)}$ corresponds to a soft-label (i.e., probabilities). We use equations 9 and 10 for proposing a new barycenter strategy between labeled point clouds, shown in algorithm 1.

Differentiation. For calculating derivatives of $\mathbf{x}_i^{(B)}$ and $\mathbf{y}_i^{(B)}$ w.r.t. $\mathbf{x}_l^{(P_k)}$, $\mathbf{y}_l^{(P_k)}$, and α , we use the Envelope theorem of [27]. In other words, we do not propagate derivatives through the iterations of algorithm 1. We provide further details in our appendix.

Computational Complexity. Let \hat{P}_k have n points in its support, for $k = 1, \dots, K$. The complexity of algorithm 1 is dominated by line 6, which has complexity $\mathcal{O}(n^3 \log n)$. Hence, the overall computational complexity is $\mathcal{O}(N_{itb} K n^3 \log n)$.

4.2 Dataset Dictionary Learning for MSDA

In this section, we introduce our novel framework, called DaDiL, and explore how to use it for MSDA. Let $\mathcal{Q} = \{\hat{Q}_{S_\ell}\}_{\ell=1}^{N_S} \cup \{\hat{Q}_T\}$ correspond to N_S labeled sources and an unlabeled target. Let $\mathcal{A} = [\alpha_1, \dots, \alpha_{N_S}, \alpha_{N_S+1}]$, and $\mathcal{P} = \{\hat{P}_k\}_{k=1}^K$. The \hat{P}_k 's are an empirical approximation of the point clouds that interpolate distributional shift. Following our notation, $\alpha_T := \alpha_{N_S+1}$. For $N = N_S + 1$, DaDiL consists on minimizing,

$$(\mathcal{P}^*, \mathcal{A}^*) = \underset{\mathcal{P}, \mathcal{A} \in (\Delta_K)^N}{\text{argmin}} \frac{1}{N} \sum_{\ell=1}^N \mathcal{L}(\hat{Q}_\ell, \mathcal{B}(\alpha_\ell; \mathcal{P})), \quad (11)$$

where \mathcal{L} is a loss between distributions. Since the target domain is not labeled, we define,

$$\mathcal{L}(\hat{Q}_\ell, \hat{B}_\ell) = \begin{cases} W_c(\hat{Q}_\ell, \hat{B}_\ell), & \text{if } \hat{Q}_\ell \text{ is labeled,} \\ W_2(\hat{Q}_\ell, \hat{B}_\ell), & \text{otherwise,} \end{cases}$$

i.e., when no labels in \hat{Q}_ℓ are available, we minimize the standard 2-Wasserstein distance. Optimizing 11 over entire datasets might be intractable due the complexity of OT. We thus employ mini-batch OT [24]. In addition, we need to enforce the constraints $\mathbf{y}_l^{(P_k)} \in \Delta_{n_c}$ and $\alpha_\ell \in \Delta_K$. In the first case we do a change of variables, and optimize the logits $\mathbf{p} \in \mathbb{R}^{n_c}$ s.t. $\mathbf{y} = \text{softmax}(\mathbf{p})$. In the second case, we project α_ℓ into the simplex orthogonally,

$$\text{proj}_{\Delta_K}(\alpha_\ell) = \underset{\alpha \in \Delta_K}{\text{argmin}} \|\alpha - \alpha_\ell\|_2.$$

The overall optimization algorithm is shown in algorithm 2.

Algorithm 1 Labeled Wasserstein Barycenter

Input: $\{\mathbf{X}^{(P_k)}, \mathbf{Y}^{(P_k)}\}_{k=1}^K$, $\alpha \in \Delta_K$, $\tau > 0$, N_{itb} .

- 1: **for** $i = 1, \dots, n_B$ **do**
- 2: $\mathbf{x}_i^{(B)} \sim \mathcal{N}(\mathbf{0}, \mathbf{I}_d)$, $y_i^{(B)} = \text{randint}(n_c)$
- 3: **end for**
- 4: **while** $|J_{it} - J_{it-1}| \geq \tau$ and $it \leq N_{itb}$ **do**
- 5: **for** $k = 1, \dots, K$ **do**
- 6: $\pi^{(k,it)} = \text{OT}\left((\mathbf{X}^{(P_k)}, \mathbf{Y}^{(P_k)}); (\mathbf{X}_{it}^{(B)}, \mathbf{Y}_{it}^{(B)})\right)$
- 7: **end for**
- 8: $J_{it} = \sum_{k=1}^K \alpha_k \langle \pi^{(k,it)}, \mathbf{C}^{(k)} \rangle_F$
- 9: $\mathbf{X}_{it+1}^{(B)} = \sum_{k=1}^K \alpha_k T_{\pi^{(k,it)}}(\mathbf{X}_{it}^{(B)})$
- 10: $\mathbf{Y}_{it+1}^{(B)} = \sum_{k=1}^K \alpha_k T_{\pi^{(k,it)}}(\mathbf{Y}_{it}^{(B)})$
- 11: **end while**

Output: Labeled barycenter support $(\mathbf{X}^{(B)}, \mathbf{Y}^{(B)})$.

Algorithm 2 DaDiL learning loop.

Input: $\mathcal{Q} = \{\hat{Q}_\ell\}_{\ell=1}^N$, number of iterations N_{iter} , of atoms K , of batches M , batch size n_b , learning rate η .

- 1: Initialize $\mathbf{x}_j^{(P_k)} \sim \mathcal{N}(0, \mathbf{I}_d)$, $\mathbf{a}_\ell \sim \mathcal{N}(0, \mathbf{I}_K)$.
- 2: **for** $it = 1 \dots, N_{iter}$ **do**
- 3: **for** $batch = 1, \dots, M$ **do**
- 4: **for** $\ell = 1, \dots, (N_S + 1)$ **do**
- 5: Sample $\{\mathbf{x}_1^{(Q_\ell)}, \dots, \mathbf{x}_{n_b}^{(Q_\ell)}\}$.
- 6: **if** \hat{Q}_ℓ is labeled **then**
- 7: Sample $\{\mathbf{y}_1^{(Q_\ell)}, \dots, \mathbf{y}_{n_b}^{(Q_\ell)}\}$.
- 8: **end if**
- 9: **for** $k = 1, \dots, K$ **do**
- 10: sample $\{(\mathbf{x}_1^{(P_k)}, \mathbf{p}_1^{(P_k)}), \dots, (\mathbf{x}_{n_b}^{(P_k)}, \mathbf{p}_{n_b}^{(P_k)})\}$,
- 11: change variables $\mathbf{y}_j^{(P_k)} = \text{softmax}(\mathbf{p}_j^{(P_k)})$
- 12: **end for**
- 13: calculate $\mathbf{X}^{(B_\ell)}, \mathbf{Y}^{(B_\ell)} = \mathcal{B}(\alpha_\ell; \mathcal{P})$
- 14: **end for**
- 15: $L = (1/N) \sum_{\ell=1}^N \mathcal{L}(\hat{Q}_\ell, \hat{B}_\ell)$
- 16: $\mathbf{x}_j^{(P_k)} \leftarrow \mathbf{x}_j^{(P_k)} - \eta \partial L / \partial \mathbf{x}_j^{(P_k)}$
- 17: $\mathbf{p}_j^{(P_k)} \leftarrow \mathbf{p}_j^{(P_k)} - \eta \partial L / \partial \mathbf{p}_j^{(P_k)}$
- 18: $\alpha_\ell \leftarrow \text{proj}_{\Delta_K}(\alpha_\ell - \eta \partial L / \partial \alpha_\ell)$.
- 19: **end for**
- 20: **end for**

Output: Dictionary \mathcal{P}^* and weights \mathcal{A}^* .

Intuition. We learn how to express each distribution $\hat{Q}_\ell \in \mathcal{Q}$ as a barycenter of free distributions $\mathcal{P} = \{\hat{P}_k\}_{k=1}^K$, parametrized by their support i.e., $(\mathbf{X}^{(P_k)}, \mathbf{Y}^{(P_k)})$. In other words, we learn \mathcal{P} s.t. \mathcal{Q} is contained in the *Wasserstein hull* of atoms, $\mathcal{M}(\mathcal{P})$.

Implementation. We implement algorithms 1 and 2 using Pytorch [28] and Python Optimal Transport (POT) [29], for automatic differentiation and OT details respectively. As previous works [4, 6], DaDiL is applied to the latent space of an encoder, pre-trained on source domain data, as shown in figure 1.

Computational Complexity. In algorithm 2, the complexity of line 13 dominates over other lines. As we discussed in section 4.1, the complexity of calculating $\mathcal{B}(\alpha_\ell; \mathcal{P})$ depends on the size of distributions support. Since we do computations using mini-batches, this corresponds to $\mathcal{O}(N_{itb} n_b^3 \log n_b)$. This is repeated for $N_{iter} \times M \times (N_S + 1)$, which implies a complexity of $\mathcal{O}(N_{iter} M N_S N_{itb} n_b^3 \log n_b)$.

Multi-Source Domain Adaptation. We recast the hypothesis in eq. 5 for MSDA. We assume the existence of $K > 1$ unknown distributions, P_1, \dots, P_K for which Q_ℓ can be approximated as their interpolation in Wasserstein space, i.e. $Q_\ell = T_\# B_\ell$, and $Q_\ell(Y|X) = B_\ell(Y|T(X))$, for $B_\ell = \mathcal{B}(\alpha_\ell; \mathcal{P})$ and a possibly non-linear transformation T . If $W_c(Q_\ell, B_\ell) \approx 0$ we can assume $T(\mathbf{x}) = \mathbf{x}$.

We start by learning $(\mathcal{P}, \mathcal{A})$, as illustrated in figure 2.

Then, we propose 2 ways of using our dictionary for MSDA. Our first strategy, called DaDiL-R, consists on computing $\hat{B}_T = \mathcal{B}(\alpha_T; \mathcal{P})$, i.e., the distribution in $\mathcal{M}(\mathcal{P})$ closest to \hat{Q}_T . Since each \hat{P}_k has a labeled support, algorithm 1 yields

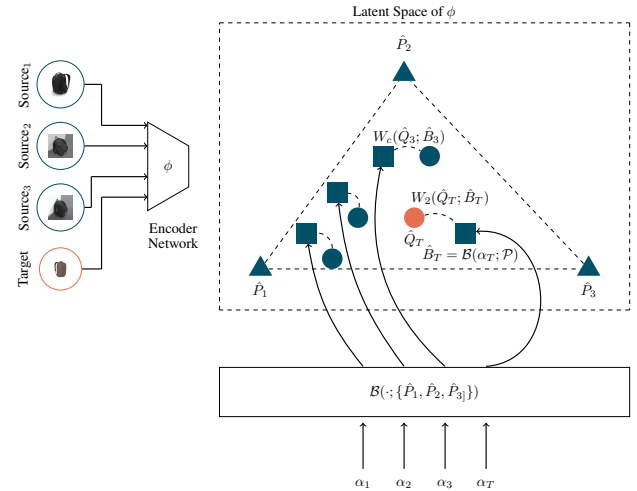


Figure 1: Conceptual illustration of DaDiL. Each domain is denoted by a blue or orange circle, corresponding to whether it is labeled or not. DaDiL *reconstructs* domains as Wasserstein barycenters, denoted by squares, of atoms, denoted by triangles. The target domain (orange circle) is unlabeled, but we are able to represent it through a labeled distribution through a Wasserstein barycenter.

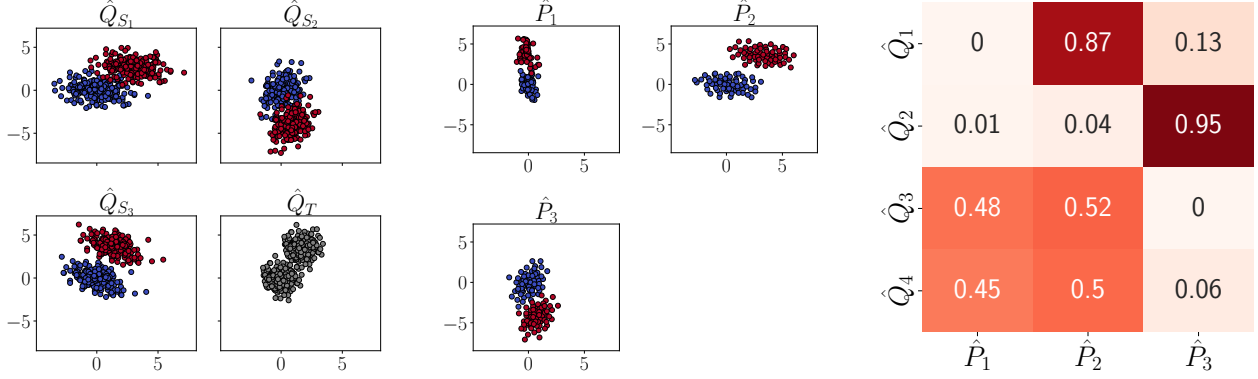


Figure 2: From left to right: set of datasets $\mathcal{Q} = \{\hat{Q}_{S_1}, \hat{Q}_{S_2}, \hat{Q}_{S_3}, \hat{Q}_T\}$, where \hat{Q}_T is the unlabeled target domain; atoms $\mathcal{P} = \{\hat{P}_1, \hat{P}_2, \hat{P}_3\}$; barycentric weights \mathcal{A} .

matrices $\mathbf{X}^{(B_T)}$ and $\mathbf{Y}^{(B_T)}$ corresponding to the support of \hat{B}_T . Then,

$$\hat{h}_R = \operatorname{argmin}_{h \in \mathcal{H}} \hat{\mathcal{R}}_{B_T}(h) = \frac{1}{n} \sum_{i=1}^n \mathcal{L}(h(\mathbf{x}_i^{(B_T)}), y_i^{(B_T)})$$

We theoretically justify it using Theorem 2 of [9],

Theorem 1. (Due to [9]) Let $\mathbf{X}^{(P)} \in \mathbb{R}^{n_P \times d}$ and $\mathbf{X}^{(Q)} \in \mathbb{R}^{n_Q \times d}$ be i.i.d. samples from P and Q . Then, for any $d' > d$ and $\xi' < \sqrt{2}$ there exists some constant n_0 depending on d' s.t. for $\delta \in (0, 1)$ and $\min(n_P, n_Q) \geq n_0 \max(\delta^{-(d+2)}, 1)$ with probability at least $1 - \delta$ for all h ,

$$\mathcal{R}_Q(h) \leq \mathcal{R}_P(h) + W_2(\hat{P}, \hat{Q}) + \zeta + \lambda,$$

where,

$$\zeta = \sqrt{2(\log 1/\delta)/\xi'} \left(\sqrt{1/n_P} + \sqrt{1/n_Q} \right),$$

$$\lambda = \min_{h \in \mathcal{H}} \mathcal{R}_Q(h) + \mathcal{R}_P(h).$$

Additional discussion on this result is provided in our appendix. We apply this result for the residual shift $W_2(\hat{Q}_T, \hat{B}_T)$,

$$\mathcal{R}_{Q_T}(h) \leq \mathcal{R}_{B_T}(h) + W_2(\hat{Q}_T, \hat{B}_T) + \zeta + \lambda. \quad (12)$$

As discussed in [9], 3 factors play a role in the success of DA, namely, $W_2(\hat{P}, \hat{Q})$, $\mathcal{R}_{B_T}(h)$, and λ . The first term is the reconstruction error, and is directly minimized in algorithm 2. The second term is the risk of h in B_T , which is minimized when learning the classifier $\hat{h}_R = \operatorname{argmin}_{h \in \mathcal{H}} \mathcal{R}_{B_T}(h)$. This term depends on the separability of classes in \hat{B}_T , which is enforced by considering labels in the ground-cost (eqn. 9). The last term is the joint risk λ of a classifier learned with data from Q_T and B_T . This term is difficult to bound, as no labels in \hat{Q}_T are available, but, under the hypothesis $Q_T(Y|X) = B_T(Y|T(X))$, this term is low. This was similarly assumed by [1, 9]. DaDiL-R is illustrated in figure 3a.

Our second strategy, called DaDiL-E, is based on ensembling. Since each of our atoms is labeled, i.e., each $\mathbf{x}_i^{(P_k)}$ has an associated $\mathbf{y}_i^{(P_k)}$, we may learn a set of K classifiers, $\hat{h}_k = \operatorname{argmin}_{h \in \mathcal{H}} \hat{\mathcal{R}}_{P_k}(h)$, one for each atom. Naturally, one may use $\alpha \in \Delta_K$ for weighting predictions of atom classifiers. We weight the \hat{h}_k 's using α_T , which is theoretically justified in theorem 2,

$$\hat{h}_E(\mathbf{x}_j^{(Q_T)}) = \sum_{k=1}^K \alpha_{T,k} \hat{h}_k(\mathbf{x}_j^{(Q_T)}),$$

Theorem 2. Let $\{\mathbf{X}^{(P_k)}\}_{k=1}^K$, $\mathbf{X}^{(P_k)} \in \mathbb{R}^{n_k \times d}$ and $\mathbf{X}^{(Q_T)} \in \mathbb{R}^{n_T \times d}$ be i.i.d. samples from P_k and Q_T . Let \hat{h}_k be the minimizer of \mathcal{R}_{P_k} and $\mathcal{R}_\alpha(h) = \sum_{k=1}^K \alpha_k \mathcal{R}_{P_k}(h)$. Under the same conditions of theorem 1, and for $\delta \in (0, 1)$, with

probability at least $1 - \delta$, the following holds,

$$\begin{aligned} \mathcal{R}_{Q_T}(\hat{h}_\alpha) &\leq \mathcal{R}_\alpha(\hat{h}_\alpha) + W_2(\mathcal{B}(\alpha; \mathcal{P}), \hat{Q}_T) + \gamma + \lambda + \zeta, \\ \gamma &= \sum_{k=1}^K \alpha_k W_2(\hat{P}_k, \mathcal{B}(\alpha; \mathcal{P})), \\ \zeta &= \sum_{k=1}^K \alpha_k \sqrt{2 \log 1/\delta / \xi'} \left(\sqrt{1/n_k} + \sqrt{1/n_T} \right), \\ \lambda &= \sum_{k=1}^K \alpha_k \left(\min_{h \in \mathcal{H}} \mathcal{R}_{P_k}(h) + \mathcal{R}_{Q_T}(h) \right). \end{aligned}$$

We provide the proof of this result and additional discussion in our appendix. This bound depends on different terms. First, γ is, for a given α , minimal, as $\mathcal{B}(\alpha; \mathcal{P})$ is the minimizer of $\hat{B} \mapsto \sum_k \alpha_k W_2(\hat{P}_k, \hat{B})$. λ corresponds to the complexity of domain adaptation, and in general cannot be directly controlled due the unavailability of labels in \hat{Q}_T . Finally, ξ corresponds to the sample complexity of estimating $W_2(\hat{P}_k, Q_T)$ via finite samples. Note that α_T minimizes the terms in the r.h.s., as, by design, it minimizes the term $\alpha \mapsto W_2(\mathcal{B}(\alpha; \mathcal{P}), \hat{Q}_T)$. DaDiL-E is illustrated in figure 3b.

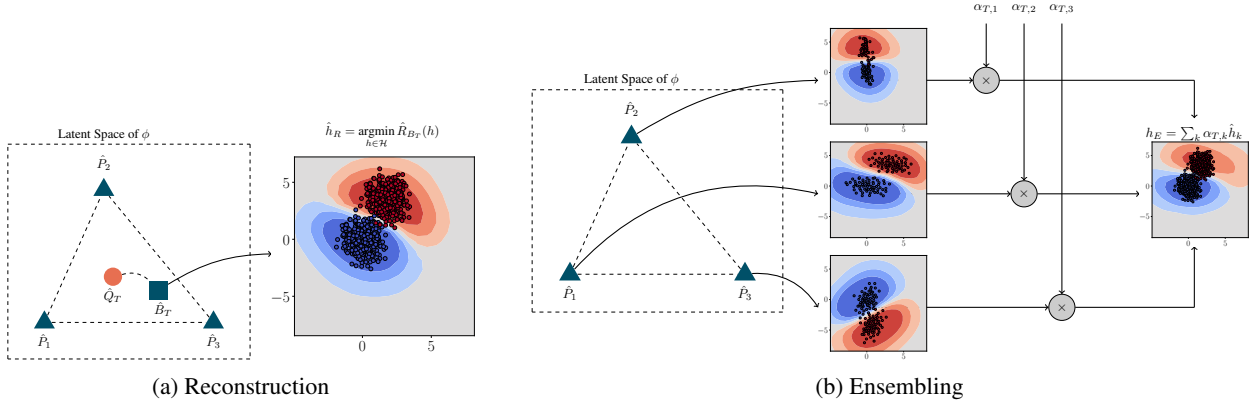


Figure 3: Conceptual illustration of the 2 methods, based on DaDiL, for MSDA.

5 Experiments

5.1 Multi-Source Domain Adaptation

Experimental Setup. All experiments were run on a computer with a Ubuntu 22.04 OS, a 12th Gen Intel(R) Core™ i9-12900H CPU with 64 GB of RAM, and with a NVIDIA RTX A100 GPU with 4GB of VRAM. We explore the following hyper-parameters,

- Number of samples n is searched among $\{50, 100, 200\} \times n_c$.
- Number of atoms K is searched among $\{3, 4, \dots, 8\}$.
- Batch size n_b is searched among $\{5, 10, 20\} \times n_c$. We further sample balanced batches from the sources.

The complexity of our model is controlled through n and K . We provide further analysis on the robustness w.r.t. hyper-parameter choice, as well as the full set of chosen hyper-parameters in our appendix. For other algorithms from the State-of-the-Art (SOTA), we use the best hyper-parameter settings reported by their respective authors.

Caltech-Office 10 is a benchmark consisting on the intersection of the Caltech 256 dataset of [30] and the Office 31 dataset of [31]. It has 4 domains: Amazon (A), dSLR (D), Webcam (W) and Caltech (C). In this benchmark we compare DaDiL with other shallow DA algorithms, such as: (i) Subspace Alignment (SA) of [32]; (ii) Transfer Component Analysis (TCA) of [33]; (iii) Optimal Transport Domain Adaptation (OTDA) of [1]; (iv) Wasserstein Barycenter Transport (WBT) of [4, 5]; (v) Weighted JDOT (WJDOT) of [6]. (i) and (ii) are standard algorithms in DA, (iii) is

Table 2: Classification accuracy (in %) of DA methods. Each column represents a target domain for which we report mean \pm standard deviation over 5 folds. * and \dagger denote results from [4] and [6].

Method	A	D	W	C	Avg
Baseline	90.55 \pm 1.36	96.83 \pm 1.33	88.36 \pm 1.33	82.95 \pm 1.26	89.67
SA	88.61 \pm 1.72	92.08 \pm 3.82	79.33 \pm 3.67	73.00 \pm 2.31	83.26
TCA*	86.83 \pm 4.71	89.32 \pm 1.33	97.51 \pm 1.18	80.79 \pm 2.65	88.61
OTDA	88.26 \pm 1.36	90.41 \pm 3.86	88.09 \pm 3.80	83.02 \pm 1.67	87.44
WJDOT \dagger	94.23 \pm 0.90	100.00 \pm 0.00	89.33 \pm 2.91	85.93 \pm 2.07	92.37
WBT $^*_{reg}$	92.74 \pm 0.45	95.87 \pm 1.43	96.57 \pm 1.76	85.01 \pm 0.84	92.55
DaDiL-R	94.06 \pm 1.82	<u>98.75 \pm 1.71</u>	<u>98.98 \pm 1.51</u>	<u>88.97 \pm 1.06</u>	<u>95.19</u>
DaDiL-E	<u>94.16 \pm 1.58</u>	100.00 \pm 0.00	99.32 \pm 0.93	89.15 \pm 1.68	95.66

Table 3: Classification accuracy (in %) of DA methods. \mathcal{P} and \mathcal{A} indicate learning atom distributions and barycentric coefficients respectively. T indicates an additional transport step towards \hat{Q}_T .

Method	\mathcal{P}	\mathcal{A}	T	A	D	W	C	Avg.
WB				88.54 \pm 1.16	90.62 \pm 8.38	93.89 \pm 3.30	83.73 \pm 1.49	89.19
WBT $_{reg}$			✓	92.74 \pm 0.45	95.87 \pm 1.43	96.57 \pm 1.76	85.01 \pm 0.84	92.55
WBR-R		✓		91.35 \pm 1.19	91.87 \pm 9.47	81.69 \pm 3.26	86.31 \pm 1.73	86.09
WBR-E		✓		91.97 \pm 2.40	91.87 \pm 2.79	83.73 \pm 2.57	86.13 \pm 1.84	88.42
DaDiL-R	✓	✓		<u>94.06 \pm 1.82</u>	<u>98.75 \pm 1.71</u>	<u>98.98 \pm 1.51</u>	<u>88.97 \pm 1.06</u>	<u>95.19</u>
DaDiL-E	✓	✓		94.16 \pm 1.58	100.00 \pm 0.00	99.32 \pm 0.93	89.15 \pm 1.68	95.66

the single-source OT baseline, and (iv, v) are the SOTA for shallow MSDA. The baseline corresponds to training a single-layer Perceptron with the concatenation of source domain data.

Our results is presented in table 2. DaDiL improve over previous OT-based MSDA baselines, i.e. WJDOT and WBT, being especially better on the Webcam and Caltech domains. Overall, we improve previous SOTA by 3.15 in terms of average DA performance.

Ablation Study. We investigate the effectiveness of DiL in comparison with other barycenter-based approaches. As follows, we compare the performance on the Caltech-Office 10 benchmark of 4 methods: (i) Wasserstein Barycenter (WB); (ii) WBT; (iii) Wasserstein Barycentric Coordinates Regression (WBR)-R and WBR-E, which can be understood as the adaptation of the framework of [34] for point clouds. The R and E methods are analogous to DaDiL when the atoms are initialized and fixed as the source domains. We provide further details of this adaptation in our appendix.

We report our findings in table 3. Overall, WB and WBR have sub-optimal performance. On the one hand, this implies that $\hat{Q}_T \notin \mathcal{M}(\mathcal{Q}_S)$. On the other hand, this implies that DiL is key for MSDA. Indeed, since $\hat{P}_k \in \mathcal{P}$ are free, DaDiL learns \mathcal{P} s.t. $\hat{Q}_T \in \mathcal{M}(\mathcal{P})$. WBT $_{reg}$ compensates this fact by transporting the \hat{B} towards \hat{Q}_T , thus minimizing the residual shift $W_2(\hat{B}, \hat{P}_T)$.

Refurbished Office 31. In this experiment, we use the Office 31 benchmark of [31], with the improvements proposed by [35]. This benchmark has 3 domains: Amazon (A), dSLR (D) and Webcam (W). Our goal is to establish a comparison with deep DA methods. As follows, we consider: (i) Domain Adversarial Neural Network (DANN) of [12], (ii) Wasserstein Distance Guided Representation Learning (WDGRL) of [13], (iii) Deep-JDOT of [3], (iv) Moment Matching for MSDA (M3SDA) of [14], (v) WJDOT and (vi) WBT. While (i) - (iii) are single source baselines, (iv) is a standard method for MSDA. We use a ResNet-50 [36] as backbone.

A summary of our results is shown in table 4. Overall, DaDiL-R and E are especially better than previous algorithms in the Amazon domain. As a consequence, in terms of average domain performance, DaDiL-R and E improve over the second-best method (WBT $_{reg}$) by a margin of 2.29% and 1.37% respectively.

CWRU. In this benchmark, we explore DaDiL for cross-domain fault diagnosis. The goal is to classify which type of fault has occurred, based on sensor readings. Hence, we extract 2048 Fourier coefficients from a sub-set of 4096 time-steps extracted from the raw signals (see [37], or our appendix for more details). As feature extractor, we use a 3-layer fully connected encoder. We compare 3 single, and 5 multi-source DA algorithms to DaDiL, namely, DANN, OTDA, TCA, M3SDA, LTC-MSDA of [38], JCPOF of [26], WBT $_{reg}$ and WJDOT.

Table 4: Classification accuracy (in %) of DA methods on the Refurbished Office 31 benchmark. Each column represents a target domain for which we report mean \pm standard deviation over 5 folds.

Method	A	D	W	Avg
Baseline	70.57	97.00	95.47	87.68
DANN	78.19	97.00	93.08	89.42
WDGRL	76.06	97.00	93.71	88.92
DeepJDOT	80.85	94.00	93.38	89.61
M3SDA	64.89	98.00	<u>96.85</u>	86.58
WBT _{reg}	77.48	96.00	95.59	89.69
WJDOT	70.21	97.00	94.96	87.39
DaDiL-R	85.46	93.00	97.48	91.98
DaDiL-E	<u>83.51</u>	94.00	94.34	<u>90.61</u>

Table 5: Classification accuracy (in %) of DA methods on the CWRU benchmark. Each column represents a target domain for which we report mean \pm standard deviation over 5 folds.

Method	1772rpm	1750rpm	1730rpm	Avg
Baseline	70.90 \pm 0.40	79.76 \pm 0.11	72.26 \pm 0.23	74.31
DANN	67.96 \pm 8.52	64.38 \pm 5.03	57.75 \pm 17.06	63.37
OTDA	70.48 \pm 2.25	79.61 \pm 0.25	74.98 \pm 1.26	75.02
TCA	87.17 \pm 4.25	84.11 \pm 4.77	92.74 \pm 4.12	88.01
M3SDA	56.86 \pm 7.31	69.81 \pm 0.36	61.06 \pm 6.35	62.57
WJDOT	65.01 \pm 0.27	69.81 \pm 0.07	57.40 \pm 1.18	64.07
M3SDA _{β}	60.15 \pm 8.38	70.00 \pm 0.00	64.00 \pm 5.47	64.72
LTC-MSDA	82.21 \pm 8.03	75.33 \pm 5.91	81.04 \pm 5.45	79.52
JCPOT	77.48 \pm 0.86	<u>96.00 \pm 0.10</u>	95.59 \pm 0.56	91.74
WBT _{reg}	<u>99.28 \pm 0.18</u>	79.91 \pm 0.04	97.71 \pm 0.76	92.30
DaDiL-R	99.86 \pm 0.21	99.85 \pm 0.08	100.00 \pm 0.00	99.90
DaDiL-E	93.71 \pm 6.50	83.63 \pm 4.98	<u>99.97 \pm 0.05</u>	<u>92.33</u>

We present a summary of our results in table 5. Overall, WBT_{reg} and DaDiL are the best performing methods, demonstrating the power of Wasserstein barycenters for DA. Our method outperforms WBT_{reg} by 7.71%, in terms of average domain performance. Furthermore, our methods surpass other deep learning baselines, such as M3SDA [14] and LTC-MSDA [38], by a margin of 19.90%.

5.2 Domain Adaptation using Atom Interpolations

Besides performing MSDA with optimal barycentric coordinates $\alpha_T \in \Delta_K$, in this section we explore the question *how well do $\alpha \in \Delta_K$ perform?* We explore these questions in terms of Wasserstein distance $W_2(\mathcal{B}(\alpha; \mathcal{P}), \hat{Q}_T)$, and classification accuracy of using α in DaDiL-R and E, as shown in figure 4.

In figure 4 we construct an uniform grid over Δ_3 . For each α in such grid, we reconstruct $\mathcal{B}(\alpha; \mathcal{P})$, then we evaluate: (i) the *reconstruction loss* $W_2(\mathcal{B}(\alpha; \mathcal{P}), \hat{Q}_T)$; (ii) the classification accuracy of DaDiL-E, with α , on \hat{Q}_T ; (iii) the classification accuracy of DaDiL-R with α , on \hat{Q}_T . These correspond to the 3 rows in figure 4. As shown, the weights found by DaDiL are optimal w.r.t. other choices $\alpha \in \Delta_3$. Nonetheless, a wide region of the simplex yield *equally good* reconstructions, either w.r.t. reconstruction loss, or w.r.t. DA performance. We conclude that DaDiL is able to learn distribution whose interpolations generalize well to the target domain.

Furthermore, in figure 5 we analyze the correlation between DA performance and reconstruction loss, for $\alpha \in \Delta_3$. Our analysis shows that these 2 terms are negatively correlated, for both DaDiL-R and E. Indeed, based on our theoretical analysis (theorems 1 and 2), classification risk is bounded by the reconstruction loss. Since DA performance is inversely proportional to the classifier risk in a given domain, our analysis agrees with both theorems.

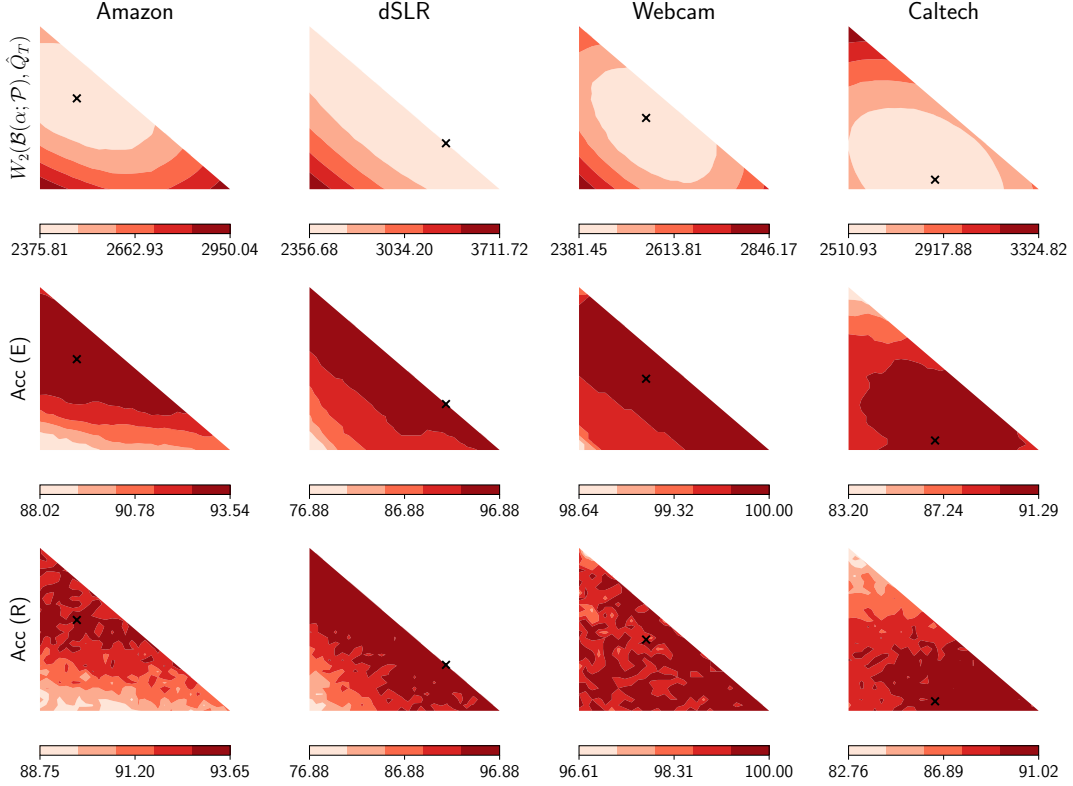


Figure 4: Analysis of DA on Caltech-Office with interpolations of dictionary atoms. The black cross represents the α found by DaDiL.

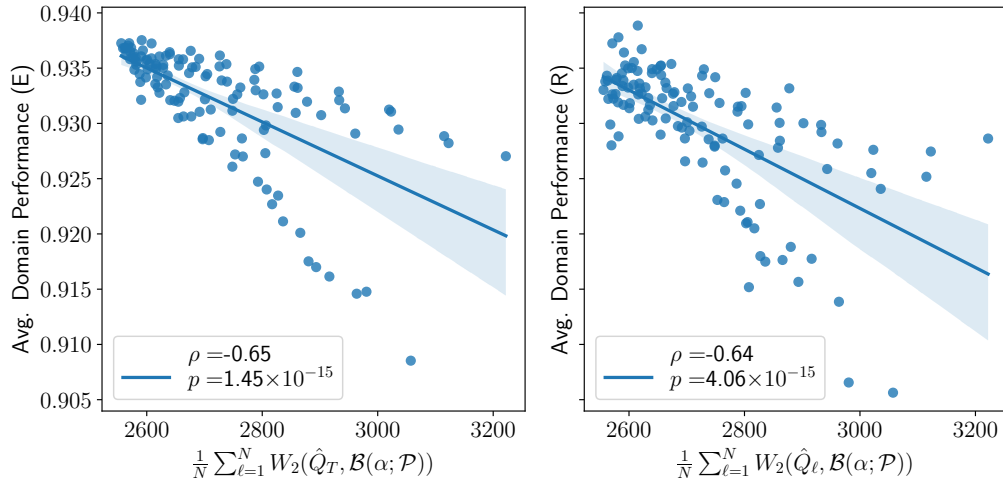


Figure 5: Correlation between DiL loss and the performance of DaDiL-R and E.

Finally, we analyze the performance of DaDiL-R and E for α taken uniformly from Δ_K , for $K \in \{3, \dots, 8\}$. We report our findings in figure 6, and compare the performance w.r.t. DaDiL performance in table 2, for $\alpha := \alpha_T$. As shown in Figure 6 α_T is above average for most domains and number of atoms K .

Overall, figures 4, 5 and 6 show that DaDiL learns an optimal set of barycentric coordinates for the target domain. Nonetheless, interpolations in the Wasserstein hull $\mathcal{M}(\mathcal{P})$ of atom distributions can be equally interesting for MSDA. These remarks indicate that DaDiL is able to (i) learn common discriminant information about the source domains; (ii) interpolate the distributional shift between the various distributions in $\mathcal{Q} = \{\hat{Q}_{S_\ell}\}_{\ell=1}^{N_S} \cup \{\hat{Q}_T\}$ through the atoms \mathcal{P} .

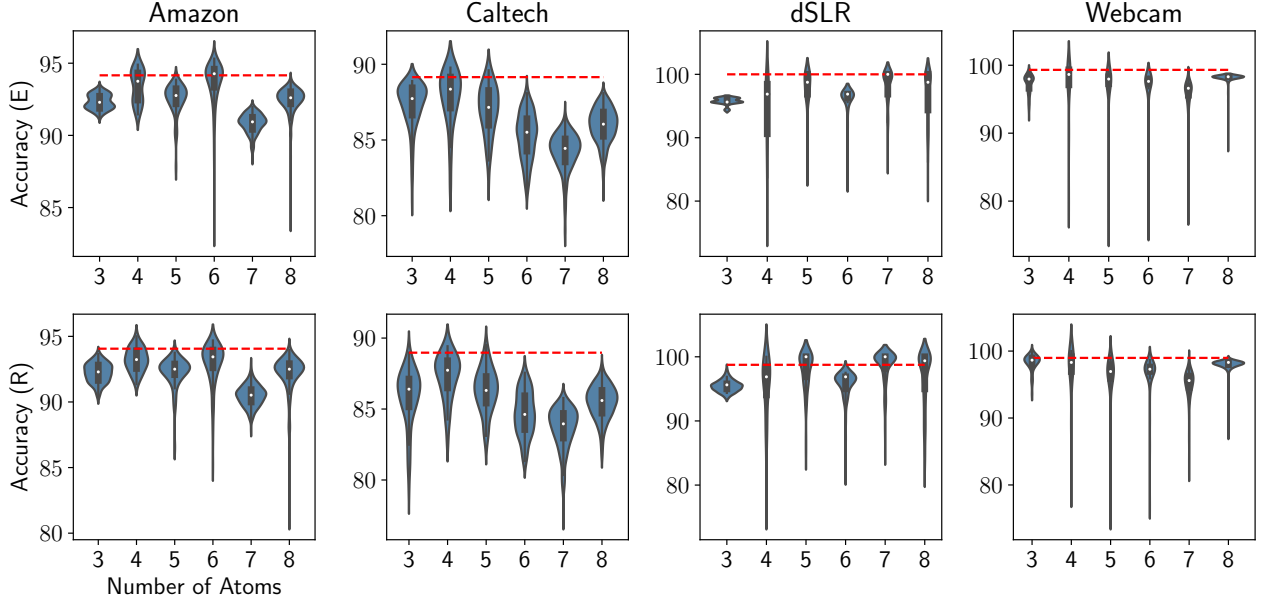


Figure 6: Performance analysis of latent space interpolations on the Caltech-Office 10 benchmark. The red dotted line corresponds to the results reported in Table 2 for DaDiL.

6 Discussion

Benefits of Dictionary Learning. Our proposed framework allows for the learning of new, *virtual distributions*, which can then be used to reconstruct distributions seen during DiL by generating new samples. As such, our algorithm is able to improve over past SOTA, and, as shown in section 5.2, we are able to generate new domains by interpolating the atom distributions in Wasserstein space. Especially, we improve previous SOTA and barycenter-based algorithms by 3.15% in the Caltech-Office 10 benchmark.

Benefits of Wasserstein Barycenters. In our experiments, we established a comparison between DaDiL, WBT [4] and WJDOT [6]. The first two methods rely on Wasserstein barycenters for reconstructing the target domain, while WJDOT aggregates the source domains linearly. Overall we show that Wasserstein barycenters are an important component of MSDA, as they allow to *average probability distributions non-linearly*. On the other hand, the linear average of distributions can be understood as importance weighting on samples. Under the covariate shift hypothesis, re-weighting samples is enough, but under more complicated shifts (i.e. non-linear data transformations), Wasserstein barycenters are more flexible.

Shallow vs. Deep Domain Adaptation. As remarked by [6], the assumption of having a meaningful feature extractor ϕ before performing DA is realistic, as in modern practice pre-trained models are widely available. It is noteworthy that a fine-tuning step with source-domain data may be necessary in order to achieve better performance. In addition, doing so allows for the comparison with deep DA methods. In this context, we remark that our method improves over previous deep DA SOTA in the context of the Refurbished Office 31 and CWRU benchmarks. Overall, shallow DA is computationally simpler than deep DA, as one needs to learn a smaller set of parameters (i.e., the classification layer).

7 Conclusion

In this work, we tackle the problem of MSDA through OT-based DiL of probability distributions. We view elements in DiL as empirical distributions. As such we learn a dictionary that is able to interpolate the distributional shift of distributions in DiL. We make 2 methodological contributions to MSDA, through methods called DaDiL-R, based on the reconstruction of labeled samples in the target domain, and DaDiL-E, based on ensembling of atom classifiers. Our methods are theoretically grounded on previous theorems from the literature [9, Theorem 2] and a novel result (theorem 2).

Our proposed methods are compared to 11 methods from the SOTA in MSDA in 3 benchmarks, namely, Caltech-Office 10 [31, 30], Refurbished Office 31 [31, 35] and CWRU. We improve previous performance by 3.15%, 2.29% and 7.71%

respectively. Moreover, we show that general interpolations in the Wasserstein hull of our learned dictionary can be equally interesting for MSDA.

Our framework opens an interesting line of research, for *learning* empirical distributions, generating synthetic through Wasserstein barycenters and interpolating distributional shift in Wasserstein space. It is flexible so as to accommodate other notions of barycenters of distributions, and loss functions between reconstructions and real datasets. In practical terms, future works will focus on parametric formulations of DaDiL. In theoretical terms, we seek to understand the statistical challenges posed by DaDiL.

References

- [1] Nicolas Courty, Rémi Flamary, Devis Tuia, and Alain Rakotomamonjy. Optimal transport for domain adaptation. *IEEE transactions on pattern analysis and machine intelligence*, 39(9):1853–1865, 2016.
- [2] Nicolas Courty, Rémi Flamary, Amaury Habrard, and Alain Rakotomamonjy. Joint distribution optimal transportation for domain adaptation. *Advances in Neural Information Processing Systems*, 30, 2017.
- [3] Bharath Bhushan Damodaran, Benjamin Kellenberger, Rémi Flamary, Devis Tuia, and Nicolas Courty. Deepjdot: Deep joint distribution optimal transport for unsupervised domain adaptation. In *Proceedings of the European Conference on Computer Vision (ECCV)*, pages 447–463, 2018.
- [4] Eduardo Fernandes Montesuma and Fred Maurice Ngole Mboula. Wasserstein barycenter for multi-source domain adaptation. In *Proceedings of the IEEE/CVF Conference on Computer Vision and Pattern Recognition (CVPR)*, pages 16785–16793, June 2021.
- [5] Eduardo Fernandes Montesuma and Fred Maurice Ngole Mboula. Wasserstein barycenter transport for acoustic adaptation. In *ICASSP 2021 - 2021 IEEE International Conference on Acoustics, Speech and Signal Processing (ICASSP)*, pages 3405–3409, May 2021.
- [6] Rosanna Turrise, Rémi Flamary, Alain Rakotomamonjy, et al. Multi-source domain adaptation via weighted joint distributions optimal transport. In *The 38th Conference on Uncertainty in Artificial Intelligence*, 2022.
- [7] Antoine Rolet, Marco Cuturi, and Gabriel Peyré. Fast dictionary learning with a smoothed wasserstein loss. In *Artificial Intelligence and Statistics*, pages 630–638. PMLR, 2016.
- [8] Morgan A Schmitz, Matthieu Heitz, Nicolas Bonneel, Fred Ngole, David Coeurjolly, Marco Cuturi, Gabriel Peyré, and Jean-Luc Starck. Wasserstein dictionary learning: Optimal transport-based unsupervised nonlinear dictionary learning. *SIAM Journal on Imaging Sciences*, 11(1):643–678, 2018.
- [9] Ievgen Redko, Amaury Habrard, and Marc Sebban. Theoretical analysis of domain adaptation with optimal transport. In *Joint European Conference on Machine Learning and Knowledge Discovery in Databases*, pages 737–753. Springer, 2017.
- [10] Masashi Sugiyama, Matthias Krauledat, and Klaus-Robert Müller. Covariate shift adaptation by importance weighted cross validation. *Journal of Machine Learning Research*, 8(5), 2007.
- [11] Sinno Jialin Pan and Qiang Yang. A survey on transfer learning. *IEEE Transactions on knowledge and data engineering*, 22(10):1345–1359, 2009.
- [12] Yaroslav Ganin, Evgeniya Ustinova, Hana Ajakan, Pascal Germain, Hugo Larochelle, François Laviolette, Mario Marchand, and Victor Lempitsky. Domain-adversarial training of neural networks. *The journal of machine learning research*, 17(1):2096–2030, 2016.
- [13] Jian Shen, Yanru Qu, Weinan Zhang, and Yong Yu. Wasserstein distance guided representation learning for domain adaptation. In *Proceedings of the AAAI Conference on Artificial Intelligence*, volume 32, 2018.
- [14] Xingchao Peng, Qinxun Bai, Xide Xia, Zijun Huang, Kate Saenko, and Bo Wang. Moment matching for multi-source domain adaptation. In *Proceedings of the IEEE/CVF international conference on computer vision*, pages 1406–1415, 2019.
- [15] De-An Huang and Yu-Chiang Frank Wang. Coupled dictionary and feature space learning with applications to cross-domain image synthesis and recognition. In *Proceedings of the IEEE international conference on computer vision*, pages 2496–2503, 2013.
- [16] Marco Cuturi. Sinkhorn distances: Lightspeed computation of optimal transport. *Advances in neural information processing systems*, 26, 2013.
- [17] Vladimir Vapnik. Principles of risk minimization for learning theory. *Advances in neural information processing systems*, 4, 1991.

- [18] Ievgen Redko, Emilie Morvant, Amaury Habrard, Marc Sebban, and Younès Bennani. A survey on domain adaptation theory: learning bounds and theoretical guarantees. *arXiv preprint arXiv:2004.11829*, 2020.
- [19] Eduardo Fernandes Montesuma, Fred Ngole Mboula, and Antoine Souloumiac. Recent advances in optimal transport for machine learning. *arXiv preprint arXiv:2306.16156*, 2023.
- [20] Gabriel Peyré, Marco Cuturi, et al. Computational optimal transport: With applications to data science. *Foundations and Trends® in Machine Learning*, 11(5-6):355–607, 2019.
- [21] Filippo Santambrogio. Optimal transport for applied mathematicians. *Birkäuser, NY*, 55(58-63):94, 2015.
- [22] Martial Agueh and Guillaume Carlier. Barycenters in the wasserstein space. *SIAM Journal on Mathematical Analysis*, 43(2):904–924, 2011.
- [23] Marco Cuturi and Arnaud Doucet. Fast computation of wasserstein barycenters. In *International conference on machine learning*, pages 685–693. PMLR, 2014.
- [24] Kilian Fatras, Younes Zine, Szymon Majewski, Rémi Flamary, Rémi Gribonval, and Nicolas Courty. Minibatch optimal transport distances; analysis and applications. *arXiv preprint arXiv:2101.01792*, 2021.
- [25] David Alvarez-Melis and Nicolo Fusi. Geometric dataset distances via optimal transport. *Advances in Neural Information Processing Systems*, 33:21428–21439, 2020.
- [26] Ievgen Redko, Emilie Morvant, Amaury Habrard, Marc Sebban, and Younes Bennani. *Advances in domain adaptation theory*. Elsevier, 2019.
- [27] SN Afriat. Theory of maxima and the method of lagrange. *SIAM Journal on Applied Mathematics*, 20(3):343–357, 1971.
- [28] Adam Paszke, Sam Gross, Francisco Massa, Adam Lerer, James Bradbury, Gregory Chanan, Trevor Killeen, Zeming Lin, Natalia Gimelshein, Luca Antiga, Alban Desmaison, Andreas Kopf, Edward Yang, Zachary DeVito, Martin Raison, Alykhan Tejani, Sasank Chilamkurthy, Benoit Steiner, Lu Fang, Junjie Bai, and Soumith Chintala. Pytorch: An imperative style, high-performance deep learning library. In H. Wallach, H. Larochelle, A. Beygelzimer, F. d'Alché-Buc, E. Fox, and R. Garnett, editors, *Advances in Neural Information Processing Systems 32*, pages 8024–8035. Curran Associates, Inc., 2019.
- [29] Rémi Flamary, Nicolas Courty, Alexandre Gramfort, Mokhtar Z Alaya, Aurélie Boisbunon, Stanislas Chambon, Laetitia Chapel, Adrien Corenflos, Kilian Fatras, Nemo Fournier, et al. Pot: Python optimal transport. *J. Mach. Learn. Res.*, 22(78):1–8, 2021.
- [30] Gregory Griffin, Alex Holub, and Pietro Perona. Caltech-256 object category dataset. Technical report, California Institute of Technology, 2007.
- [31] Kate Saenko, Brian Kulis, Mario Fritz, and Trevor Darrell. Adapting visual category models to new domains. In *European conference on computer vision*, pages 213–226. Springer, 2010.
- [32] Basura Fernando, Amaury Habrard, Marc Sebban, and Tinne Tuytelaars. Unsupervised visual domain adaptation using subspace alignment. In *Proceedings of the IEEE international conference on computer vision*, pages 2960–2967, 2013.
- [33] Sinno Jialin Pan, Ivor W Tsang, James T Kwok, and Qiang Yang. Domain adaptation via transfer component analysis. *IEEE transactions on neural networks*, 22(2):199–210, 2010.
- [34] Nicolas Bonneel, Gabriel Peyré, and Marco Cuturi. Wasserstein barycentric coordinates: histogram regression using optimal transport. *ACM Trans. Graph.*, 35(4):71–1, 2016.
- [35] Tobias Ringwald and Rainer Stiefelwagen. Adaptiope: A modern benchmark for unsupervised domain adaptation. In *Proceedings of the IEEE/CVF Winter Conference on Applications of Computer Vision*, pages 101–110, 2021.
- [36] Kaiming He, Xiangyu Zhang, Shaoqing Ren, and Jian Sun. Deep residual learning for image recognition. In *Proceedings of the IEEE conference on computer vision and pattern recognition*, pages 770–778, 2016.
- [37] Bo Zhang, Wei Li, Xiao-Li Li, and See-Kiong Ng. Intelligent fault diagnosis under varying working conditions based on domain adaptive convolutional neural networks. *Ieee Access*, 6:66367–66384, 2018.
- [38] Hang Wang, Minghao Xu, Bingbing Ni, and Wenjun Zhang. Learning to combine: Knowledge aggregation for multi-source domain adaptation. In *Computer Vision—ECCV 2020: 16th European Conference, Glasgow, UK, August 23–28, 2020, Proceedings, Part VIII 16*, pages 727–744. Springer, 2020.
- [39] Cédric Villani. *Optimal transport: old and new*, volume 338. Springer, 2009.
- [40] Shai Ben-David, John Blitzer, Koby Crammer, Alex Kulesza, Fernando Pereira, and Jennifer Wortman Vaughan. A theory of learning from different domains. *Machine learning*, 79(1):151–175, 2010.

- [41] François Bolley, Arnaud Guillin, and Cédric Villani. Quantitative concentration inequalities for empirical measures on non-compact spaces. *Probability Theory and Related Fields*, 137(3-4):541–593, 2007.
- [42] Jean Feydy, Thibault Séjourné, François-Xavier Vialard, Shun-ichi Amari, Alain Trounev, and Gabriel Peyré. Interpolating between optimal transport and mmd using sinkhorn divergences. In *The 22nd International Conference on Artificial Intelligence and Statistics*, pages 2681–2690. PMLR, 2019.
- [43] Michael Held, Philip Wolfe, and Harlan P Crowder. Validation of subgradient optimization. *Mathematical programming*, 6(1):62–88, 1974.
- [44] Laurent Condat. Fast projection onto the simplex and the ℓ_1 ball. *Mathematical Programming*, 158(1):575–585, 2016.
- [45] Kilian Fatras, Younes Zine, Rémi Flamary, Rémi Gribonval, and Nicolas Courty. Learning with minibatch wasserstein: asymptotic and gradient properties. In *AISTATS*, 2020.

A Introduction

We divide our supplementary material into 3 sections. In appendix B we provide further details about our theoretical results. Especially, appendix B.2 we provide a proof for our theorem 2. In appendix C we provide a detailed description of our adaptation of the WBR algorithm of [34]. This algorithm allows us to establish an illustration on *why perform dictionary learning*, as learning atom distributions improves over simply regressing barycentric coordinates of the Wasserstein hull of source distributions \mathcal{Q}_S . Finally, appendix E provides further experimentation on the hyper-parameters of our algorithm. We provide in table 13 the complete setting of hyper-parameters used in our experiments.

B Proofs of Theorems

B.1 Preliminaries and Theorem 1

In the following discussion, we need to extend the definition of risk of a classifier h , for pairs $(h, h') \in \mathcal{H}$, as is done in [9],

$$h^* = \operatorname{argmin}_{h \in \mathcal{H}} \mathcal{R}_Q(h, h') = \mathbb{E}_{\mathbf{x} \sim Q} [\mathcal{L}(h(\mathbf{x}), h'(\mathbf{x}))].$$

This is different to what was presented in section 3.1, but is needed to state the results that follow. Note that, under the assumption that \mathcal{L} suffices the triangle inequality, so does \mathcal{R}_Q for $h_1, h_2, h_3 \in \mathcal{H}$. We start by bounding risks under P and Q by their Wasserstein distance.

Lemma 1. (Due to [9]) *Let P and Q be two probability distributions over \mathbb{R}^d . Assume that the cost function $c(\mathbf{x}^{(P)}, \mathbf{x}^{(Q)}) = \|\phi(\mathbf{x}^{(P)}) - \phi(\mathbf{x}^{(Q)})\|_{\mathcal{F}}$, where \mathcal{F} is a reproducing kernel Hilbert space equipped with kernel $\Phi : \mathbb{R}^d \times \mathbb{R}^d \rightarrow \mathbb{R}$ induced by $\phi : \mathbb{R}^d \rightarrow \mathcal{H}_k$ and $\Phi(\mathbf{x}^{(P)}, \mathbf{x}^{(Q)}) = \langle \phi(\mathbf{x}^{(P)}), \phi(\mathbf{x}^{(Q)}) \rangle_{\mathcal{F}}$. Assume that the kernel $\Phi \in \mathcal{F}$ is square-root integrable w.r.t. both P and Q and $0 \leq \Phi(\mathbf{x}^{(P)}, \mathbf{x}^{(Q)}) \leq M, \forall \mathbf{x}^{(P)}, \mathbf{x}^{(Q)} \in \mathbb{R}^d$. Then the following holds,*

$$\mathcal{R}_Q(h, h') \leq \mathcal{R}_P(h, h') + W_1(P, Q). \tag{13}$$

Note. Following [39], Hölder’s inequality implies that $p \leq q \implies W_p \leq W_q$, where W_p corresponds to the Wasserstein distance with ground-cost $c(\mathbf{x}^{(P)}, \mathbf{x}^{(Q)}) = \|\mathbf{x}^{(P)} - \mathbf{x}^{(Q)}\|_p^p$. As consequence, bound 13 is also valid for the Euclidean distance.

The consequence of Lemma 1 relates the risk of a pair (h, h') under distributions P and Q by the Wasserstein distance. This is in line with other theoretical results, such as [40]. Before relating the risks of h with the *empirical Wasserstein distance*, one needs to establish the convergence of the empirical \hat{P} to the true P . This is done in the next lemma.

Lemma 2. (Due to [41]) *Let P be a probability distribution over \mathbb{R}^d , so that for some $\alpha > 0$ we have that $\int_{\mathbb{R}^d} e^{\alpha \|\mathbf{x}\|^2} dP < \infty$ and \hat{P} be its associated empirical approximation with support $\{\mathbf{x}_i^{(P)}\}_{i=1}^n$ drawn independently from P . Then, for any $d' > d$ and $\xi' < \sqrt{2}$ there is a constant n_0 depending on d' and some square exponential moment of P such that for any $\epsilon > 0$ and $n \geq n_0 \max(\epsilon^{-(d'+2)}, 1)$,*

$$\mathbb{P}[W_1(\hat{P}, P) > \epsilon] \leq \exp\left(-\frac{\xi'}{2} n \epsilon^2\right),$$

where d' and ξ' can be calculated explicitly.

Lemma 2 states the conditions for which \hat{P} and P are close in the sense of Wasserstein. This last bound is on the form $\mathbb{P}[\text{quantity} > \epsilon] < \delta$, that is, with high probability $\text{quantity} \leq \epsilon$. These types of bounds are ubiquitous in the theoretical analysis of learning algorithms. We can express ϵ explicitly in terms of δ ,

$$\epsilon = \sqrt{\frac{2}{n\xi'} \log\left(\frac{1}{\delta}\right)}, \quad (14)$$

which will be useful in the following discussion. We recall that, as stated in [9, Theorem 2], and Theorem 1, under suitable conditions,

$$\begin{aligned} \mathcal{R}_Q(h) &\leq \mathcal{R}_P(h) + W_2(\hat{P}, \hat{Q}) + \zeta + \lambda, \\ \zeta &= \sqrt{2^{(\log 1/\delta)}/\xi'} \left(\sqrt{1/n_P} + \sqrt{1/n_Q} \right), \\ \lambda &= \min_{h \in \mathcal{H}} \mathcal{R}_Q(h) + \mathcal{R}_P(h), \end{aligned}$$

These results allowed [9] to provide theoretical guarantees for the OTDA framework of [1]. As discussed in [9], the minimization of $W_2(\hat{P}, \hat{Q})$ alone does not guarantee DA success. As illustrated by the authors, during transportation one can minimize the domain distance while mixing classes. This leads to a situation where one has a low W_2 , but a risk \mathcal{R}_P high over all $h \in \mathcal{H}$. The same reasoning may be applied to the joint error λ . A few assumptions need to be done at this point,

- H1 The distribution \hat{P}' which reduces $W_2(\cdot, \hat{Q})$ has distinguishable classes, i.e., $\mathcal{R}_{P'}(h)$ is low.
- H2 The distribution \hat{P}' which reduces $W_2(\cdot, \hat{Q})$ has the same class-structure as \hat{Q} (i.e. classes lie on the same side of the boundary). In other words, λ is low.

We now recast this theorem and hypothesis in terms of DaDiL-R. First, one has $Q = Q_T$, i.e., the target domain distribution. Second, one uses $P = B_T$, i.e., the barycentric reconstruction of the target, through our dictionary. Our algorithm regulates \mathcal{R}_{B_T} by integrating the labels in the ground-cost. As a consequence, giving mass to samples with different classes is too costly, and the OT transport plans are *class sparse*, i.e. $\pi_{ij} > 0 \iff y_i^{(P)} = y_j^{(Q)}$.

The second hypothesis is difficult to ensure in unsupervised DA, as one does not have any information about the class structure of \hat{Q} . As [1] and [9], we assume a degree of regularity in the distributional shift of distributions in \mathcal{Q} . This allows us to predict classes in the target, through label propagation.

B.2 Proof of Theorem 2

Before proving our results, we define the following risks,

$$\begin{aligned} \mathcal{R}_{Q_T}(h) &= \mathbb{E}_{\mathbf{x} \sim Q_T} [\mathcal{L}(h(\mathbf{x}), h_{Q_T,0}(\mathbf{x}))], \\ \mathcal{R}_{P_k}(h) &= \mathbb{E}_{\mathbf{x} \sim P_k} [\mathcal{L}(h(\mathbf{x}), h_{P_k,0}(\mathbf{x}))], \\ \mathcal{R}_\alpha(h) &= \sum_{k=1}^K \alpha_k \mathcal{R}_{P_k}(h). \end{aligned}$$

which are the risk under the target, under each of the atom distributions, and the combined risk weighted by α , respectively. $h_{Q_T,0}$ and $h_{P_k,0}$ are the ground-truth labeling functions of the target distribution, and atom k . Likewise, we define the following classifiers,

$$\begin{aligned} h_{T,k}^* &= \operatorname{argmin}_{h \in \mathcal{H}} \mathcal{R}_{Q_T}(h) + \mathcal{R}_{P_k}(h), \\ \hat{h}_k &= \operatorname{argmin}_{h \in \mathcal{H}} \mathcal{R}_{P_k}(h), \\ \hat{h}_\alpha(\mathbf{x}) &= \sum_k \alpha_k \hat{h}_k(\mathbf{x}). \end{aligned}$$

Our proof relies on the triangle inequality for the risk. With our previous definitions,

$$\mathcal{R}_{Q_T}(\hat{h}_\alpha) \leq \mathcal{R}_{Q_T}(h_{T,k}^*) + \mathcal{R}_{Q_T}(h_{T,k}^*, \hat{h}_\alpha).$$

Now, we add and subtract $\mathcal{R}_{P_k}(h_{T,k}^*, \hat{h}_\alpha)$,

$$\begin{aligned} \mathcal{R}_{Q_T}(\hat{h}_\alpha) &\leq (\mathcal{R}_{Q_T}(h_{T,k}^*, \hat{h}_\alpha) - \mathcal{R}_{P_k}(h_{T,k}^*, \hat{h}_\alpha)) + (\mathcal{R}_{Q_T}(h_{T,k}^*) + \underbrace{\mathcal{R}_{P_k}(h_{T,k}^*, \hat{h}_\alpha)}_{\leq \mathcal{R}_{P_k}(h_{T,k}^*) + \mathcal{R}_{P_k}(\hat{h}_\alpha)}), \\ &\leq \underbrace{(\mathcal{R}_{Q_T}(h_{T,k}^*, \hat{h}_\alpha) - \mathcal{R}_{P_k}(h_{T,k}^*, \hat{h}_\alpha))}_{\leq W_2(P_k, Q_T) \text{ by Lemma 1.}} + \underbrace{(\mathcal{R}_{Q_T}(h_{T,k}^*) + \mathcal{R}_{P_k}(h_{T,k}^*))}_{=\lambda_k \text{ by Def.}} + \mathcal{R}_{P_k}(\hat{h}_\alpha) \end{aligned}$$

where, in the first line, we used the triangle inequality again. This result leads to,

$$\mathcal{R}_{Q_T}(\hat{h}_\alpha) \leq \mathcal{R}_{P_k}(\hat{h}_\alpha) + W_2(P_k, Q_T) + \lambda_k.$$

Now, summing over k , weighted by α , one has $\mathcal{R}_{Q_T}(\hat{h}_\alpha) = \sum_k \alpha_k \mathcal{R}_{Q_T}(\hat{h}_\alpha)$. We can bound this latter term as follows,

$$\begin{aligned} \sum_k \alpha_k \mathcal{R}_{Q_T}(\hat{h}_\alpha) &\leq \sum_k \alpha_k \mathcal{R}_{P_k}(\hat{h}_\alpha) + \sum_k \alpha_k (W_2(P_k, Q_T) + \lambda_k), \\ &= \mathcal{R}_\alpha(\hat{h}_\alpha) + \sum_k \alpha_k (W_2(P_k, Q_T) + \lambda_k), \\ &\leq \mathcal{R}_\alpha(\hat{h}_\alpha) + \sum_k \alpha_k (W_2(\hat{P}_k, \hat{Q}_T) + \lambda_k + \zeta_k), \end{aligned} \tag{15}$$

From this last inequality, we use the triangle inequality between \hat{P}_k , $\mathcal{B}(\alpha; \mathcal{P})$ and \hat{Q}_T ,

$$W_2(\hat{P}_k, \hat{Q}_T) \leq W_2(\hat{P}_k, \mathcal{B}(\alpha; \mathcal{P})) + W_2(\mathcal{B}(\alpha; \mathcal{P}), \hat{Q}_T).$$

Summing over k , and noting that,

$$\sum_k \alpha_k W_2(\mathcal{B}(\alpha; \mathcal{P}), \hat{Q}_T) = W_2(\mathcal{B}(\alpha; \mathcal{P}), \hat{Q}_T)$$

one has,

$$\sum_k \alpha_k W_2(\hat{P}_k, \hat{Q}_T) \leq W_2(\mathcal{B}(\alpha; \mathcal{P}), \hat{Q}_T) + \gamma.$$

Plugging this result back into equation 15,

$$\mathcal{R}_{Q_T}(\hat{h}_\alpha) \leq \mathcal{R}_\alpha(\hat{h}_\alpha) + W_2(\hat{Q}_T, \mathcal{B}(\alpha; \mathcal{P})) + \gamma + \lambda + \zeta,$$

where,

$$\gamma = \sum_{k=1}^K \alpha_k W_2(\hat{P}_k, \mathcal{B}(\alpha; \mathcal{P})), \text{ and, } \lambda = \sum_{k=1}^K \alpha_k \lambda_k, \xi = \sum_{k=1}^K \alpha_k \xi_k$$

which concludes the proof.

This theorem is similar to previous theoretical guarantees for MSDA, such as those of [40], [9], and [4]. A few remarks may be made about the terms γ , λ and ζ ,

- ζ corresponds to the sample complexity of approximating $W_2(P_k, Q_T)$ by $W_2(\hat{P}_k, \hat{Q}_T)$. It decreases with the number of samples in the atoms, and in the target domain.
- λ corresponds to the domain adaptation complexity between the atoms and the target. As in DaDiL-R, this term cannot be bounded, but it is in general assumed to remain bounded during DA.
- γ is a new term, corresponding to $\sum_k \alpha_k W_2(\hat{P}_k, \mathcal{B}(\alpha; \mathcal{P}))$. For a given α , this term is minimal since $\mathcal{B}(\alpha; \mathcal{P})$ is, by definition, the minimizer of $\hat{B} \mapsto \sum_k \alpha_k W_2(\hat{P}_k, \hat{B})$.

C Wasserstein Barycentric Coordinate Regression

In this section we describe how to adapt the WBR algorithm [34] for empirical distributions. Let $\mathcal{Q}_S = \{\hat{Q}_\ell\}_{\ell=1}^{N_S}$ be the set of labeled source distributions, and $\alpha \in \Delta_{N_S}$ be a set of *barycentric coordinates*, i.e., they allow to interpolate between distributions in \mathcal{Q} through $\mathcal{B}(\alpha; \mathcal{Q}_S)$. Let \hat{Q}_T be an unlabeled target distribution. [34] proposed regressing α by the following minimization problem,

$$\alpha^* = \underset{\alpha \in \Delta_{N_S}}{\operatorname{argmin}} W_2(\hat{Q}_T, \mathcal{B}(\alpha; \mathcal{Q}_S)). \quad (16)$$

In [34], the minimization in equation 16 was done when \hat{Q}_{S_ℓ} and \hat{Q}_T are histograms, i.e., vectors in Δ_d . In our case, these distributions are empirical. As a consequence, we can employ a similar method to DaDiL for regressing $\alpha \in \Delta_{N_S}$, as shown in algorithm 3.

Algorithm 3 Wasserstein Barycentric Regression of Point Clouds.

Input: $\mathcal{Q}_S = \{\hat{Q}_{S_\ell}\}_{\ell=1}^{N_S}$, \hat{Q}_T , batch size n_b , learning rate η , number of iterations N_{iter} , number of batches M .

- 1: Initialize $\alpha_\ell = N_S^{-1}$, $\ell = 1, \dots, N_S$.
- 2: **for** $it = 1 \dots, N_{iter}$ **do**
- 3: **for** $batch = 1, \dots, M$ **do**
- 4: **for** $\ell = 1, \dots, N_S$ **do**
- 5: Sample $\mathbf{X}^{(Q_{S_\ell})} = \{\mathbf{x}_i^{(Q_{S_\ell})}\}_{i=1}^{n_b}$
- 6: **end for**
- 7: sample $\mathbf{X}^{(Q_T)} = \{\mathbf{x}_j^{(Q_T)}\}_{j=1}^{n_b}$
- 8: calculate $\mathbf{X}^{(B)} = \mathcal{B}(\alpha_\ell; \mathcal{Q}_S)$
- 9: $L \leftarrow W_2(\hat{Q}_T, \hat{B})$
- 10: $\alpha \leftarrow \operatorname{proj}_{\Delta_{N_S}}(\alpha - \eta \partial L / \partial \alpha_\ell)$.
- 11: **end for**
- 12: **end for**

Output: Barycentric coordinates α^* .

As noted by [34], the barycentric regression algorithm leads to poor reconstructions, when \hat{Q}_T is far from the distributions in \mathcal{Q}_S . This remark explains its sub-optimal performance in our ablation study (i.e., table 3 of our main paper). These results also support why DiL is important in MSDA, as learning atom distributions leads to a Wasserstein hull \mathcal{P} for which \hat{Q}_T is close.

D Experiments Details

D.1 Dataset Description

Caltech-Office 10: We use the experimental setting of [4], namely, the 5 fold cross-validation partitions and the features (DeCAF 7th layer activations).

Refurbished-Office 31: This dataset consists on the Office 31 dataset of [31]. We follow the discussion of [35] and adopt their modifications, namely, the replacements of images in the Amazon domain that contained label noise. The authors modifications are publicly available in a Gitlab repository². Since our method relies on features, we adopt the following methodology,

1. A backbone deep Neural Net (NN) is fitted using all source data. For instance if adaptation is done between $A, D \rightarrow W$, then all data from A and D is used for training the NN.
2. Features are extracted using the convolutional layers. This generates a new dataset of shape $(n_{samples}, d)$, where d is the dimensionality of features.

We split each domain in a train and test set, corresponding to 80% and 20% of samples, respectively. This is shown in Table 7. Here, we highlight that during fine-tuning in step 1, all data from sources is used (i.e., training and test partitions), as evaluation is performed solely on target data. DaDiL is then run using the features extracted at step 2. For the Refurbished-Office 31, we chose to use the ResNet-50 of [36] as backbone.

²<https://gitlab.com/tringwald/adaptiope>

Since this benchmark has a significant performance saturation (i.e., fine-tuning a complete ResNet yields 100% classification accuracy when adapting towards *dSLR* and *Webcam*), we use a slightly more challenging setting, where we keep all but the last convolutional block frozen during fine-tuning.

CWRU: The third benchmark we experiment on is the Case Western Reserve University bearing fault diagnosis benchmark, which is publicly available³. We use the 12k drive end bearing fault data, where we consider the file ids reported in table 6. This is similar to other studies in bearing fault diagnosis, as reported in [37].

Table 6: File ids of data used in the CWRU experiments.

Label	0	1	2	3	4	5	6	7	8	9
Fault Location	None	Inner Race Fault			Ball Fault			Outer Race Fault		
Fault Diameter		0.007	0.014	0.021	0.007	0.014	0.021	0.007	0.014	0.021
1772 rpm	98	106	170	210	119	186	223	131	198	235
1750 rpm	99	107	171	211	120	187	224	132	199	236
1730 rpm	100	108	172	212	121	188	225	133	200	237

In the CWRU benchmark, for each file id we randomly sample a window of length 4096 from the complete signal. From this sub-sample, we extract the first 2048 Fourier coefficients, from the 4096 acquires through a Fast Fourier Transform (FFT). For each target domain, we pre-train a multi-layer Perceptron⁴ from scratch, and use the activation of its penultimate layer as features for shallow methods, including DaDiL.

Overall, when training DaDiL, we use all source data (i.e. train and test), and the train partition of the target domain, without its labels. The performance evaluation is done in the independent test set, which is never seen during training.

Table 7: Details about the datasets considered for domain adaptation.

Dataset	# Classes	Domain	# Training Samples	# Test Samples	# Samples
Caltech-Office 10	10	Amazon	748	210	958
		dSLR	108	49	157
		Webcam	224	71	295
		Caltech	956	224	1180
		Total	2036	554	2590
Office 31	31	Amazon	2253	564	2817
		dSLR	398	100	498
		Webcam	636	159	795
		Total	3287	823	4110
CWRU	10	1772rpm	6000	2000	8000
		1750rpm	6000	2000	8000
		1720rpm	6000	2000	8000
		Total	18000	6000	24000

D.2 DaDiL Implementation Details

In this section we highlight a few details in our implementation. Concerning algorithm 1, we remark that we differentiate $\mathbf{X}^{(B)}$ and $\mathbf{Y}^{(B)}$ at termination of algorithm 1 (main paper). This means that derivatives are not back-propagated through the while loop in algorithm 1 (main paper). In practical terms, this corresponds to stating *with torch.no_grad()* before the loop, then using the transport plans $\pi^{(k)}$ at termination for calculating the support $\mathbf{X}^{(B)}$, $\mathbf{Y}^{(B)}$. This is similar to what was proposed by [42]. In practice, $\pi_{i,l}^{(k)}$ is not differentiated w.r.t. $\mathbf{x}_l^{(P_k)}$, $\mathbf{y}_l^{(P_k)}$ or α .

We also implement algorithm 2 using Pytorch, thus calculating the derivatives of $L(\mathcal{P}, \mathcal{A})$ automatically. The projection into the simplex is done using POT’s function *ot.utils.proj_simplex*, which does so by sorting (see e.g., [43] and [44] for more details).

³<https://engineering.case.edu/bearingdatacenter/download-data-file>

⁴2048 → 1024 → 512 → 256 with ReLU activations.

E Additional Experiments

In this section, we provide additional experiments. In section E.1, we explore the reasoning for tuning the hyper-parameters of DaDiL. In addition, section E.2 we explore the stability of algorithm 2 w.r.t. different random initializations of atoms, as well as the evolution of weights α w.r.t. iterations.

E.1 Hyper-parameter Analysis

In our experiments, we tune hyper-parameters so as to maximize performance on target domain training data. Our evaluation is done in an independent partition of the test set, not seen during training. In what follows, we highlight that previous best-performing method in the SOTA, i.e. WBT_{reg} , has 92.55% of average domain performance.

Number of Atoms. We test $K \in \{3, \dots, 8\}$. We divide our discussion into two experiments: (i) DA performance, and (ii) weight sparsity as a function of the number of atoms K . We fix $n = 1000$ and $n_b = 200$. First, we measure classification performance on the target domain, which is shown in Table 8. Performance fluctuates over choices of K , being higher with increasing number of components. For all choices, we improve over previous SOTA.

Table 8: Classification accuracy in %, as a function of number of components K .

K	3	4	5	6	7	8
DaDiL-R	93.53	94.16	93.33	94.30	94.23	95.30
DaDiL-E	93.89	94.33	93.86	94.68	94.66	95.70

Second, for a fixed K we measure the sparsity of α_T through the following score,

$$\text{sparsity score} = 100\% \times \left(1 - \frac{\|\alpha_T\|_0}{K}\right),$$

that is, the percentage of zero entries in the target domain weights.

Table 9: Sparsity Score (in %) as a function of number of atoms K .

K	3	4	5	6	7	8
Amazon	6.66	0.00	8.00	20.00	8.58	15.00
Caltech	6.66	20.00	16.00	30.00	31.42	27.50
dSLR	0.00	5.00	8.00	23.33	25.71	27.50
Webcam	6.66	5.00	12.00	10.00	20.00	27.50
Avg	5.00	7.50	11.00	20.83	21.43	24.37

As the number of atoms grows, α_T becomes more sparse. This implies that DaDiL selects a sub-set of atoms to reconstruct the target domain whenever K is overestimated.

Number of Samples. We divide our discussion into two experiments: (i) DA performance and (ii) support density, as a function of the number of samples n in the support of \hat{P}_k . We fix $K = 8$ and $n_b = 200$. First, as shown in table 10, DaDiL is more sensible to the number of samples in the support of atoms. While the best choice is $n = 1000$, for other values of n we remain SOTA.

Table 10: Classification accuracy in %, as a function of the number of samples n .

n	500	1000	2000
DaDiL-R	92.48	95.30	93.57
DaDiL-E	93.12	95.70	93.58

Second, let us explore the density of samples in the atoms support. Let $N_5(\mathbf{x}_i^{(P_k)})$ denote the set of 5 nearest neighbors in \hat{P}_k , w.r.t. $\mathbf{x}_i^{(P_k)}$. We evaluate the density of atoms support as a function of n by measuring the average distance of each point in $\mathbf{X}^{(P_k)}$ to its 5 nearest neighbors, i.e.,

$$\text{density score} = \frac{1}{5nK} \sum_{k=1}^K \sum_{i=1}^n \sum_{\mathbf{x}_j^{(P_k)} \in N_5(\mathbf{x}_i^{(P_k)})} \|\mathbf{x}_i^{(P_k)} - \mathbf{x}_j^{(P_k)}\|_2^2.$$

As table 11 shows, the samples concentrate over a region of \mathbb{R}^d , meaning that the atoms’ support are stable w.r.t n .

Table 11: Average distance to 5 nearest neighbors of points in the learned atoms support.

n	1000	2000	3000	4000
Amazon	43.28 ± 0.42	34.92 ± 1.14	33.04 ± 1.80	32.18 ± 1.45
Caltech	43.12 ± 0.60	34.49 ± 1.57	34.33 ± 2.04	32.97 ± 2.28
dSLR	43.60 ± 0.96	35.82 ± 0.39	33.03 ± 0.47	32.72 ± 0.70
Webcam	42.71 ± 1.01	36.07 ± 0.93	35.14 ± 2.69	33.45 ± 1.00
Avg	43.18	35.31	33.88	32.83

Batch size n_b . For fixed $K = 8$ and $n = 1000$, we evaluate $n_b \in \{50, 100, 200\}$ in terms of average domain performance. Our results are shown in Table 12. Note that performance increases with an increasing batch size, which agrees with previous research in mini-batch OT [45, 24]. In addition, performance is more stable w.r.t. batch size choice (e.g., compare tables 12 and 10), and DaDiL remains largely above previous SOTA for all choices of batch size.

Table 12: Classification accuracy in %, as a function of batch size n_b .

n_b	50	100	200
DaDiL-R	94.78	94.94	95.70
DaDiL-E	94.64	94.72	95.30

Learning rate and Number of iterations. Since we use large, balanced batches, our optimization problem is stable w.r.t. learning rate and number of iterations. Overall, we set η as the maximum value for which our algorithm does not diverge. DaDiL is run until reconstruction loss hits a plateau. Note that this criteria does not assumes labeled samples from the target domain.

Final Hyper-parameter Settings. Overall, we select hyper-parameters that maximize classification performance on target domain samples seen during training. For evaluation, we use an independent partition of the target domain data not seen during training. We report the used hyper-parameters in table 13.

Table 13: Final hyper-parameter settings for each benchmark.

Dataset	DaDiL-R	DaDiL-E	
Caltech-Office 10	K	8	8
	n	1000	1000
	n_b	200	200
	η	10^{-1}	10^{-1}
	N_{iter}	10	10
Refurbished Office 31	K	6	6
	n	3100	1550
	n_b	155	310
	η	5×10^{-2}	5×10^{-2}
	N_{iter}	60	60
CWRU	K	8	3
	n	1000	1000
	n_b	200	200
	η	5×10^{-2}	5×10^{-2}
	N_{iter}	60	60

E.2 Learning Loop Stability

In this section, we analyze the stability of DaDiL’s learning problem (i.e., the minimization of eqn. 11) under different initializations of atom’s support and weights. This experiment is conducted on the CWRU benchmark, where we evaluate stability w.r.t. 2 criteria,

1. The stability of the loss curve w.r.t. different and independent initializations,
2. The stability of parameter updates w.r.t. iterations,

For the first criterion, we calculate the mean and standard deviation of L_{it} over 5 independent runs. Overall, the loss is stable w.r.t. random initializations, and it converges to different local minima, as shown by the small variation in the loss at the beginning and end of training.

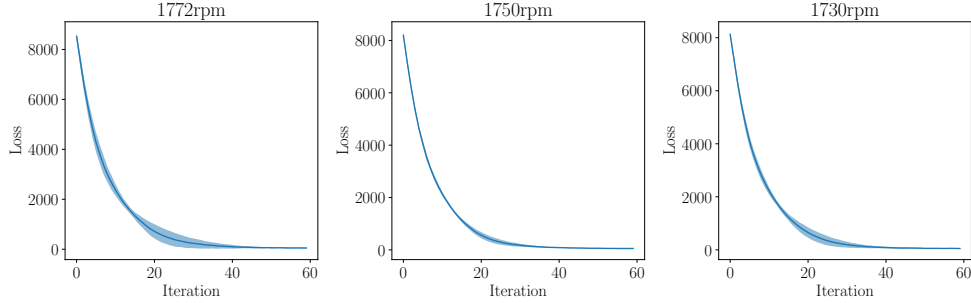


Figure 7: DaDiL’s loss function (eqn 11) as a function of iterations. The solid line represents an average over 5 independent runs, whereas the shaded region represents a confidence interval of $\pm 2\sigma$.

These experiments raise the question on whether minimizers to eqn. 11 are unique. It is generally not the case. For instance, if one wants to express $\mathcal{Q} = \{Q_0\}$, $Q_0 = \mathcal{N}(\mu, I)$ as the barycenter of $\mathcal{P} = \{P_1, P_2, P_3\}$, where $P_i = \mathcal{N}(\mu_i, I)$, any set of means with $(1/3) \sum_{i=1}^3 \mu_i = \mu$ is a minimizer of eqn. 11. Thus theoretical analysis of minimizers of eqn. 11 is challenging, and we will consider it in future works.

Concerning the second criterion, we evaluate the magnitude of updates in $\mathbf{X}_{it}^{(P_k)}$, $\mathbf{Y}_{it}^{(P_k)}$ and \mathcal{A}_{it} . We use the Frobenius norm for comparing updates, i.e.,

$$\begin{aligned} \Delta_X(it) &= \frac{1}{K} \sum_{k=1}^K \|\mathbf{X}_{it}^{(P_k)} - \mathbf{X}_{it-1}^{(P_k)}\|_F^2, \\ \Delta_Y(it) &= \frac{1}{K} \sum_{k=1}^K \|\mathbf{Y}_{it}^{(P_k)} - \mathbf{Y}_{it-1}^{(P_k)}\|_F^2, \\ \Delta_A(it) &= \|\mathcal{A}_{it} - \mathcal{A}_{it-1}\|_F^2. \end{aligned} \tag{17}$$

We show our results in figure 8. Note that, towards the end of learning, the updates on DaDiL’s variables fall close to 0, indicating that the algorithm converged to a local minimum.

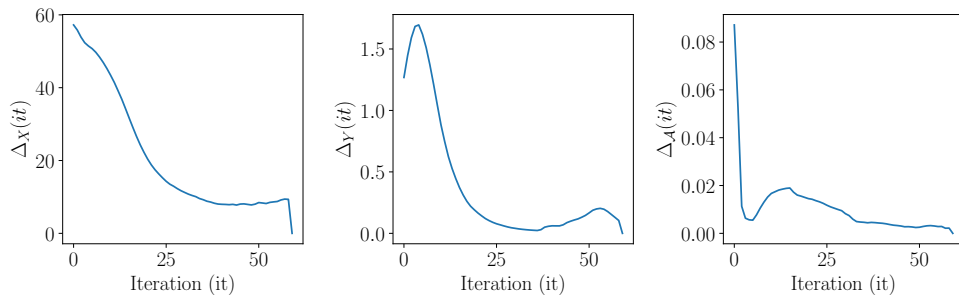


Figure 8: Magnitude of updates of DaDiL’s algorithm as a function of iterations.